O_2 *A*-band line parameters to support atmospheric remote sensing. Part II: The rare isotopologues

D. A. Long[a], D. K. Havey[b], S. S. Yu[d], M. Okumura[a], C. E. Miller[d] and J. T. Hodges[c,*]
[a]*Division of Chemistry and Chemical Engineering, California Institute of Technology, Pasadena, CA 91125, USA*
[b]*Department of Chemistry and Biochemistry, James Madison University, Harrisonburg, VA 22807, USA*
[c]*Chemical and Biochemical Reference Data Division, National Institute of Standards and Technology, 100 Bureau Drive, Gaithersburg, Maryland 20899, USA and*
[d]*Jet Propulsion Laboratory, California Institute of Technology, 4800 Oak Grove Drive, Pasadena, CA 91109, USA*
(Dated: January 10, 2011)

*Corresponding author:
Email address: joseph.hodges@nist.gov (J. T. Hodges) Tel.: +1(301)975-2605; fax: +1(301)975-3670.

Abstract

Frequency-stabilized cavity ring-down spectroscopy (FS-CRDS) was employed to measure over 100 transitions in the *R*-branch of the $b^1\Sigma_g^+ \leftarrow X^3\Sigma_g^-(0,0)$ band for the rare O_2 isotopologues. The use of ^{17}O- and ^{18}O-enriched mixtures allowed for line positions to be measured for the $^{16}O^{17}O$, $^{16}O^{18}O$, $^{17}O_2$, $^{17}O^{18}O$, and $^{18}O_2$ isotopologues. Simultaneous fits to the upper and lower states were performed for each isotopologue using the FS-CRDS positions supplemented by microwave, millimeter, submillimeter, terahertz, and Raman ground state positions from the literature. Positions, line intensities, pressure broadening parameters, and collisional narrowing parameters are reported for the $^{16}O^{18}O$ and $^{16}O^{17}O$ isotopologues which are based upon the present study and our earlier FS-CRDS work (Long et al., JQSRT, 111, 2021 and Robichaud et al., JPCA, 113, 13089). The calculated line intensities include a term for the observed Herman-Wallis-like interaction and correct a frequency-dependent error which is present in existing spectroscopic databases.

Keywords: Oxygen, *A*-band, Cavity ring-down spectroscopy, Remote Sensing, Isotopologue, Galatry profile.

1. Introduction

The O_2 *A*-band [$b^1\Sigma_g^+ \leftarrow X^3\Sigma_g^-(0,0)$] is utilized extensively in remote sensing to determine surface pressure [1-2], aerosol and cloud optical properties [3-4], cloud-top heights [5], and optical pathlength. Recent remote sensing measurements have demonstrated high precision (e.g. surface pressure determinations with a reproducibility better than 0.1% [1-2] and optical pathlength to better than 0.3% [6-7]), requiring spectroscopic parameters with even higher precision. Additionally, many *A*-band transitions from the dominant $^{16}O_2$ isotopologue are heavily saturated under atmospheric observing conditions. Also, transitions from rare O_2 isotopologues have significant absorption strengths, requiring

high-precision spectroscopic parameters for these transitions [8]. Despite the importance of O_2 rare isotopologues to remote sensing applications, only a few high resolution studies have measured rare isotopologue spectroscopic parameters.

Babcock and Herzberg performed the first quantitative analysis of $^{16}O^{17}O$ and $^{16}O^{18}O$ spectroscopic parameters using high-resolution atmospheric spectra [9]. Since these early measurements, a variety of techniques including Fourier-transform spectroscopy (FTS) [10-11], cavity ring-down spectroscopy (CRDS) [12], frequency-modulation spectroscopy (FMS) [13], and noise-immune cavity-enhanced optical heterodyne molecular spectroscopy (NICE-OHMS) [14] have been employed to measure rare isotopologue spectroscopic parameters. A major experimental challenge in these studies has been to obtain sufficient signal-to-noise in the high resolution spectra to retrieve accurate spectroscopic parameters for the rare isotopologues of O_2. See Robichaud et al. for a complete literature summary [15].

Recently, Robichaud et al. [15] used frequency-stabilized cavity ring-down spectroscopy (FS-CRDS) to perform the most precise rare isotopologue measurements of O_2 to date. These measurements were the first comprehensive study of line intensities and lineshape parameters for the $^{17}O^{18}O$ and $^{18}O_2$ isotopologues. These FS-CRDS measurements presently form the basis for the $^{16}O^{18}O$ and $^{16}O^{17}O$ transitions found in the HITRAN 2008 database [16].[1] The tuning range of the external-cavity diode laser, which was used in the Robichaud et al. FS-CRDS study [15], unfortunately limited our earlier measurements to the *P*-branch of the $b^1\Sigma_g^+ \leftarrow X^3\Sigma_g^-(0,0)$ band. The present study extends FS-CRDS measurements to the *R*-branch transitions and uses an ^{17}O-enriched sample to significantly improve the spectroscopic parameters determined for the ^{17}O isotopologues. We combine our present results with those of our earlier FS-CRDS studies [15,18] to generate a spectroscopic database for the $b^1\Sigma_g^+ \leftarrow X^3\Sigma_g^-(0,0)$ transitions of $^{16}O^{18}O$ and $^{16}O^{17}O$.

2. Experiment

The frequency-stabilized cavity ring-down spectrometer utilized for these measurements is located at the National Institute of Standards and Technology (NIST) Gaithersburg, MD and has been described in detail previously [19-20]. Briefly, FS-CRDS differs from traditional *cw*-CRDS techniques by actively stabilizing the intracavity length to an external frequency reference (in our case a co-resonant frequency-stabilized HeNe laser), which in turn eliminates drift in the cavity's comb of transmission modes. The probe laser frequency is then stepped from one TEM_{00} cavity mode to the next, resulting in an extremely linear and stable frequency axis [21]. Each of these modes is separated by the cavity free spectral range (FSR), which is typically determined to better than 1 part in 10^4. Sub-FSR frequency steps are made by shifting the HeNe laser frequency with an acousto-optic modulator in a double-pass alignment. In the present study, we used this procedure to take ½ FSR frequency steps (~100 MHz) to increase the sampling density of our measured spectra.

[1] Contrary to the description found in the HITRAN 2008 publication [16] (which states that the given transition frequencies were taken from Robichaud et al. [15]), the $^{16}O^{17}O$ transition frequencies found in HITRAN 2008 are identical to those found in HITRAN 2004 [17].

The probe laser used in the present study was an external cavity diode laser with an output power of 6-10 mW, a wavelength tuning range of 759-771 nm, and a linewidth of 300 kHz (1 s averaging time). Cavity mirrors with reflectivities of 99.98% were employed (cavity finesse ~15,000), leading to a noise-equivalent absorption coefficient of 6×10^{-10} cm^{-1} $Hz^{-1/2}$ for an acquisition rate of 20 Hz and relative uncertainty in the measured decay time of 0.1%. The reference laser was a frequency-stabilized HeNe laser with a long-term frequency uncertainty of 1 MHz (over 8 h). The cavity FSR was determined to be 201.970(10) MHz through the procedure of Lisak et al. [22].

Two isotopically enriched O_2 samples were employed for these measurements. The first was an ^{18}O-enriched sample (nominally 50% ^{18}O) which had been previously utilized in our measurements of the *P*-branch O_2 isotopologue transitions [15]. The supplier of this sample was unable to measure the isotopologue composition with sufficient accuracy for the present study. Therefore, we performed a mass spectral analysis of this sample using a double-focusing magnetic-sector mass spectrometer with electron impact ionization [15]. An ^{17}O-enriched sample (nominally 50% ^{17}O) was supplied with a mass spectral analysis and isotopologue fractions; as a result, no additional analysis was required. The analyses for both samples are given in Table 1.

Spectral scans of each of the isotopically enriched samples were performed over the *R*-branch (13125-13165 cm^{-1}) with a nominal step size of 100 MHz (~0.003 cm^{-1}). The ^{18}O-enriched sample and ^{17}O-enriched sample were scanned at 0.214 kPa (1.60 Torr) and 0.234 kPa (1.75 Torr), respectively. Pressure was measured with a NIST-calibrated capacitance diaphragm gauge having a full-scale response of 1.33 kPa (10 Torr) and a relative combined standard uncertainty less than 0.1%. The sample cell was placed within an insulated box to mitigate temperature variations. During these scans, temperatures ranged from 299.5-300.0 K as measured by a NIST-calibrated 2.4 kΩ thermistor. The temperature uncertainty in these experiments was examined in detail by Havey et al. [23] and shown to be less than 28 mK.

The importance of using a Galatry profile [24] (which accounts for collisional narrowing [25]) as opposed to a Voigt profile in quantitative measurements of line intensities and lineshape parameters of the $b^1\Sigma_g^+ \leftarrow X^3\Sigma_g^-(0,0)$ band has been demonstrated by our group and others [18,26-27]. However, for the purposes of determining the line center of isolated transitions, symmetric profiles, such as the Voigt or Galatry, yield identical positions when fit to a given set of data. Therefore, since the primary goal of the present study was to experimentally determine transition frequencies, for computational efficiency all transitions were fit with a Voigt profile.[2] Moreover, for the present case (< 0.234 kPa), collisional narrowing should be negligible (< 1 MHz) compared to the Doppler width (~ 850 MHz FWHM), thus ensuring effective equivalence between the Voigt and Galatry profiles. Importantly, our earlier FS-CRDS measurements [15,18,27] retrieved line intensities and lineshape parameters, and therefore, it was necessary to utilize the Galatry profile in those studies.

Line intensity, position, and pressure broadening coefficient were fit by least-squares minimization. For the isotopologues which did not contain ^{17}O, the Gaussian width was constrained to the theoretical Doppler width, whereas for the ^{17}O-containing isotopologues, the Gaussian width was floated to account for unresolved hyperfine

[2] No other spectroscopic line parameters determined in the present study (e.g. intensity, pressure broadening parameter) were reported or utilized in the generation of the line lists (Tables 4-5) given below.

splitting. Note that the observed hyperfine structure was the subject of a separate publication [28].

3. Results and discussion

The $b^1\Sigma_g^+ \leftarrow X^3\Sigma_g^-(0,0)$ band is triply forbidden as an electric dipole transition but occurs as a magnetic dipole transition [9]. The rotational energy levels of O_2 are commonly described by three quantum numbers: N, the orbital angular momentum; S, the spin; and J, the total angular momentum (i.e. $J=N+S$). The $X^3\Sigma_g^-$ ground state of O_2 (for $N''>0$) is split into three levels having $J''=N''-1$, N'', $N''+1$; while the upper state has only one level with $J'=N'$. The $^{16}O_2$ and $^{18}O_2$ isotopologues follow Bose-Einstein statistics and only odd levels of N'' have non-zero spin-statistical weights, whereas the other isotopologues can have any value of N''. The $b^1\Sigma_g^+ \leftarrow X^3\Sigma_g^-(0,0)$ band magnetic dipole transitions occur as doublets designated as ΔN (N'') ΔJ (J''), leading to four branches: *PP*, *PQ*, *RR*, and *RQ*.

Our previous FS-CRDS study [15] focused upon the *P*-branch (i.e. *PP* and *PQ* branches), while this study measured the *R*-branch. The *R*-branch of each isotopologue exhibits dense, overlapping rotational structure with a bandhead near 13165 cm^{-1}. Near the bandhead, the isotopologue transitions become heavily blended (especially in isotopically enriched mixtures); thus limiting the range of transitions we can measure quantitatively.

3.1. Line positions

Frequencies for the rare isotopologue transitions were measured relative to the $^{16}O_2$ positions which we recently have measured with FS-CRDS [21]. Those earlier measurements were referenced to the hyperfine components of ^{39}K; thus allowing for combined uncertainties below 1 MHz ($\sim 3\times10^{-5}$ cm^{-1}). Each rare isotopologue transition was referenced to the frequency of the nearest spectrally isolated $^{16}O_2$ transition. Rare isotopologue transition frequencies were corrected for pressure shifting using the *J*-dependent $^{16}O_2$ pressure shifts [29] since accurate pressure-shifting parameters for the rare isotopologues are not known and could not be accurately determined from the present data. This approximation should introduce negligible uncertainty since the pressure shift was only ~0.5 MHz (1.5×10^{-5} cm^{-1}) at the low pressures used in the present study. The estimated zero-pressure transition frequencies are given in the Supplementary Information (Tables S1-S5).

3.2 Line position calculations

Molecular constants for each of the rare isotopologues were then determined through a simultaneous fit to the lower ($X^3\Sigma_g^-$) and upper ($^1\Sigma_g^+$) states using SPFIT [30] and the formalism of Rouillé et al. [31]. FS-CRDS measurements (the present study and Robichaud et al. [15]) were used for the $b^1\Sigma_g^+ \leftarrow X^3\Sigma_g^-(0,0)$ band transition frequencies while lower state transition energies were further constrained by including microwave [32-36], millimeter [37-38], submillimeter [38-39], terahertz [40], and Raman [41] measurements. These global fits included a total of 127 [15,32], 203 [15,33-35,39-41], 539 [37] 98 [15,32], and 135 [15,36,38,40-41] transitions for the $^{16}O^{17}O$, $^{16}O^{18}O$, $^{17}O_2$,

$^{17}O^{18}O$, and $^{18}O_2$ isotopologues, respectively.[3] The resulting lower and upper state molecular constants and their corresponding uncertainties are given in Tables 2-3. Following HITRAN convention, lower state energies for the $^{16}O_2$ and $^{18}O_2$ are set relative to the N''=1, J''=0 level, whereas for the remaining isotopologues they are relative to the N''=0, J''=1 level. For comparison molecular constants determined in previous studies have been presented in Tables 8 and 9 of Robichaud et al. [15].

3.3 Line intensities

As was previously noted for the $^{16}O_2$ *A*-band [18], the calculated line intensities found in the HITRAN 2008 [16] and GEISA [42] databases contain an erroneous frequency dependence (note that the two databases have identical values for all included [$b^1\Sigma_g^+ \leftarrow X^3\Sigma_g^-(0,0)$] isotopologue transitions). This error masked a quadratic Herman-Wallis (HW)-like rotation-vibration interaction [43-44] which is present in numerous high-resolution studies [18,23,26-27,45-46]. An identical error is present in the $^{16}O^{18}O$ databases. The $^{16}O^{17}O$ line intensities in the databases exhibit a different, but still erroneous, frequency dependence.

Once the line intensities for the rare isotopologues are correctly calculated using the standard model of Gamache et al. [47] with the Hönl-London factors of Watson [48] and compared to the FS-CRDS measurements [15] there is evidence of a quadratic HW-like deviation. This effect, which is described by the term F_{HW}, is given by Watson [44] as:

$$F_{HW} = (1 + a_1 m + a_2 m^2)^2 \qquad (1)$$

where $m = -J''$ (*P*-branch) and $m = J''+1$ (*R*-branch). As seen in Figure 2, the HW-like interaction for the rare isotopologues is nearly identical to that observed for the $^{16}O_2$ isotopologue. It should be expected that the HW coefficients for the different isotopologues would be very similar. To first order the linear HW coefficient has a $\mu^{-1/2}$-dependence (where μ is the reduced mass), while the quadratic HW coefficient has a μ^{-1}-dependence [49-50]. As a result, in the most extreme case (i.e. $^{16}O_2$ vs. $^{18}O_2$), these coefficients would only differ by ~5% and ~12%, respectively. This subtle effect is below our instrumental sensitivity limit. Therefore, the HW coefficients determined for $^{16}O_2$ were utilized for all isotopologues when calculating intensities for our line list.

Band intensities were determined by a new fit of the measurements of Robichaud et al. [15] using the standard intensity model of Gamache et al. [47] with the quadratic HW like correction given in Eq. (1). These fitted band intensities differ by as much as 7% from those given in Robichaud et al. [15], because those were based on the erroneous *J*-dependent intensities given in HITRAN 2004 [17]. The present measured band intensities were compared to those calculated based upon the $^{16}O_2$ measurements, and as can be seen in Table 1 there are no significant differences. As a result, calculated band intensities were utilized in the line list calculations (as described subsequently) instead of those based on the Robichaud et al. measurements [15].

[3] For the rare isotopologues, the terms H and H_0 are not well constrained, resulting in the large uncertainties given. Global fits performed with these parameters fixed to zero led to similar fit residuals.

3.4. Calculated line parameters for the $^{16}O^{18}O$ and $^{16}O^{17}O$ isotopologues

We calculated HITRAN-style line parameters for the $^{16}O^{18}O$ and $^{16}O^{17}O$ isotopologues using our collected FS-CRDS measurements [15,18,23,27,29]. The results are presented in Tables 4 and 5. Transition frequencies ($\tilde{\nu}$) and lower state energies (E'') were calculated using the lower and upper state molecular constants given in Tables 2 and 3. Lower state energies are reported relative to the N''=0, J''=1 level in accordance with HITRAN convention. Hönl-London factors (L) were also calculated using these molecular constants and the formalism of Watson [48].

Band intensities were then determined by scaling the $^{16}O_2$ band intensity determined in Long et al. [18] by the natural isotopic abundance [17] as shown in Table 1 (see Calculated Band Intensities). Line intensities were then calculated using these band intensities and the standard intensity model of Gamache et al. [47] with the quadratic HW-like correction as described in Long et al. [18]. As was shown above, the rare isotopologues exhibited a similar HW deviation, thus, the HW coefficients previously determined for $^{16}O_2$ [18] were used for all of the isotopologues. Additionally, Tables 4 and 5 give calculated intensities for transitions up to J''=41 for the $^{16}O^{18}O$ and $^{16}O^{17}O$ isotopologues at T_{ref}=296 K and natural terrestrial isotopic abundance [17]. Uncertainties for these calculated intensities can be estimated based upon the experimental uncertainties given in Robichaud et al. [15]. Einstein-A coefficients were then calculated through the formalism of Gamache et al. [47] (see Eq. 2 of Long et al. [18]).

The earlier FS-CRDS study [15] revealed no discernible difference in pressure broadening for the different isotopologues. Therefore, self- and air-broadening parameters (γ) were calculated based upon the correlations recently determined for the $^{16}O_2$ isotopologue [18]. The J-dependent correlations for the collisional narrowing parameters (η) of $^{16}O_2$ [18] were mass-corrected for the rare isotopologues based upon the gas kinetic theory formulation: $\eta_{diff}=k_BT/(2\pi m_a Dp)$, where m_a and D are the absorber's mass and diffusion coefficient, respectively. Note that this mass correction is in agreement with the experimentally determined mass-dependence of the collisional narrowing parameter determined by Ritter and Wilkerson [26] and Robichaud et al. [15]. The pressure-shifting parameters (δ) for the rare isotopologues were constrained to the $^{16}O_2$ correlation [18,29] since we did not measure precise pressure shifts under the limited pressure range of the present experiment.

4. Conclusions

Frequency-stabilized cavity ring-down spectroscopy (FS-CRDS) has been used to measure R-branch transitions in the $b^1\Sigma_g^+ \leftarrow X^3\Sigma_g^-(0,0)$ band for all five rare O_2 isotopologues. This study complements our earlier work which focused on the P-branch. The combined FS-CRDS data set was employed to produce a recommended Galatry line list for the $^{16}O^{18}O$ and $^{16}O^{17}O$ isotopologues out to J'=40 and includes line positions, intensities, pressure broadening parameters, and collisional narrowing parameters. The reported line positions and molecular constants are based upon a simultaneous fit to the upper and lower states which included FS-CRDS measurements and a variety of earlier lower state measurements. The line intensity calculations included a Herman-Wallis-like

interaction and correct a frequency-dependent error which is found in present spectroscopic databases. We anticipate that the use of the reported line parameters will significantly reduce remote sensing residuals for these rare isotopologues.

Acknowledgements

David A. Long was supported by the National Defense Science and Engineering Graduate Fellowship and the National Science Foundation Graduate Fellowship. Daniel K. Havey acknowledges the support of the National Research Council as a postdoctoral fellow at the National Institute of Science and Technology (NIST), Gaithersburg, MD. Part of the research described in this paper was performed at the Jet Propulsion Laboratory, California Institute of Technology, under contract with the National Aeronautics and Space Administration (NASA). Additional support was provided by the Orbiting Carbon Observatory (OCO) project, a NASA Earth System Science Pathfinder (ESSP) mission; the NASA Upper Atmospheric Research Program grant NNG06GD88G and NNX09AE21G; and the NIST Greenhouse Gas Measurements and Climate Research Program.

Appendix A: Supplementary Material

Supplementary material associated with this article can be found in the online version at: doi:/ .

References

[1] O'Brien DM, English SA, DaCosta G. High-precision, high-resolution measurements of absorption in the oxygen A-band. J Atmos Ocean Technol 1997;14:105-19.

[2] O'Brien DM, Mitchell RM, English SA, Da Costa GA. Airborne measurements of air mass from O_2 A-band absorption spectra. J Atmos Ocean Technol 1998;15:1272-86.

[3] Badayev VV, Malkevich MS. On the possibility of determining the vertical profiles of aerosol attenuation using satellite measurements of reflected radiation in the 0.76-μm oxygen band. Izv Atmos Oceanic Phys 1978;14:722–7.

[4] Heidinger AK, Stephens GL. Molecular line absorption in a scattering atmosphere. Part II: Application to remote sensing in the O_2 A band. J Atmos Sci 2000;57:1615-34.

[5] O'Brien DM, Mitchell RM. Error estimates for retrieval of cloud-top pressure using absorption in the A-band of oxygen. J Appl Meteorol 1992;31:1179-92.

[6] Miller CE, Brown LR, Toth RA, Benner DC, Devi VM. Spectroscopic challenges for high accuracy retrievals of atmospheric CO_2 and the Orbiting Carbon Observatory (OCO) experiment. C R Phys 2005;6:876-87.

[7] Miller CE, Crisp D, DeCola PL, Olsen SC, Randerson JT, Michalak AM, Alkhaled A, Rayner P, Jacob DJ, Suntharalingam P, Jones DBA, Denning AS, Nicholls ME, Doney SC, Pawson S, Boesch H, Connor BJ, Fung IY, O'Brien D, Salawitch RJ, Sander SP, Sen B, Tans P, Toon GC, Wennberg PO, Wofsy SC, Yung YL, Law RM. Precision requirements for space-based X_{CO2} data. J Geophys Res-Atmos 2007;112:D10314.

[8] Yang Z, Wennberg PO, Cageao RP, Pongetti TJ, Toon GC, Sander SP. Ground-based photon path measurements from solar absorption spectra of the O_2 A-band. JQSRT 2005;90:309-21.

[9] Babcock HD, Herzberg L. Fine structure of the red system of atmospheric oxygen bands. Astrophys J 1948;108:167-90.

[10] Schermaul R. Transition probability and line broadening for the $b^1\Sigma_g^+(v=0)\leftarrow X^3\Sigma_g^-(v=0)$ band of the $^{16}O^{18}O$ isotopomer of oxygen. JQSRT 1999;62:181-91.

[11] Camy-Peyret C, Payan S, Jeseck P, Te Y, Hawat T. High resolution balloon-borne spectroscopy within the O_2 A-band: Observations and radiative transfer modeling. Proc Int Radiat Symp, Saint Petersburg, Russia 2000; Paper E4.

[12] Naus H, deLange A, Ubachs W. $b^1\Sigma_g^+$-$X^3\Sigma_g^-(0,0)$ band of oxygen isotopomers in relation to tests of the symmetrization postulate in $^{16}O_2$. Phys Rev A 1997;56:4755-63.

[13] Gagliardi G, Gianfrani L, Tino GM. Investigation of the $b^1\Sigma_g^+(v=0)\leftarrow X^3\Sigma_g^-(v=0)$ magnetic-dipole transitions in $^{18}O_2$. Phys Rev A 1997;55:4597-600.

[14] van Leeuwen NJ, Kjaergaard HG, Howard DL, Wilson AC. Measurement of ultraweak transitions in the visible region of molecular oxygen. J Mol Spectrosc 2004;228:83-91.

[15] Robichaud DJ, Yeung LY, Long DA, Okumura M, Havey DK, Hodges JT, Miller CE, Brown LR. Experimental line parameters of the $b^1\Sigma_g^+\leftarrow X^3\Sigma_g^-(0,0)$ band of

oxygen isotopologues at 760 nm using frequency-stabilized cavity ring-down spectroscopy. J Phys Chem A 2009;113:13089-99.

[16] Rothman LS, Gordon IE, Barbe A, Benner DC, Bernath PF, Birk M, Boudon V, Brown LR, Campargue A, Champion JP, Chance K, Coudert LH, Dana V, Devi VM, Fally S, Flaud JM, Gamache RR, Goldman A, Jacquemart D, Kleiner I, Lacome N, Lafferty WJ, Mandin JY, Massie ST, Mikhailenko SN, Miller CE, Moazzen-Ahmadi N, Naumenko OV, Nikitin AV, Orphal J, Perevalov VI, Perrin A, Predoi-Cross A, Rinsland CP, Rotger M, Simecková M, Smith MAH, Sung K, Tashkun SA, Tennyson J, Toth RA, Vandaele AC, Vander Auwera J. The HITRAN 2008 molecular spectroscopic database. JQSRT 2009;110:533-72.

[17] Rothman LS, Jacquemart D, Barbe A, Benner DC, Birk M, Brown LR, Carleer MR, Chackerian C, Chance K, Coudert LH, Dana V, Devi VM, Flaud JM, Gamache RR, Goldman A, Hartmann JM, Jucks KW, Maki AG, Mandin JY, Massie ST, Orphal J, Perrin A, Rinsland CP, Smith MAH, Tennyson J, Tolchenov RN, Toth RA, Vander Auwera J, Varanasi P, Wagner G. The HITRAN 2004 molecular spectroscopic database. JQSRT 2005;96:139-204.

[18] Long DA, Havey DK, Okumura M, Miller CE, Hodges JT. O_2 A-band line parameters to support atmospheric remote sensing. JQSRT 2010;111:2021-36.

[19] Hodges JT, Layer HP, Miller WW, Scace GE. Frequency-stabilized single-mode cavity ring-down apparatus for high-resolution absorption spectroscopy. Rev Sci Instrum 2004;75:849-63.

[20] Hodges JT, Ciurylo R. Automated high-resolution frequency-stabilized cavity ring-down absorption spectrometer. Rev Sci Instrum 2005;76:023112.

[21] Robichaud DJ, Hodges JT, Maslowski P, Yeung LY, Okumura M, Miller CE, Brown LR. High-accuracy transition frequencies for the O_2 A-band. J Mol Spectrosc 2008;251:27-37.

[22] Lisak D, Hodges JT. High-resolution cavity ring-down spectroscopy measurements of blended H_2O transitions. Appl Phys B 2007;88:317-25.

[23] Havey DK, Long DA, Okumura M, Miller CE, Hodges JT. Ultra-sensitive optical measurements of high-J transitions in the O_2 A-band. Chem Phys Lett 2009;483:49-54.

[24] Galatry L. Simultaneous effect of Doppler and foreign gas broadening on spectral lines. Phys Rev 1961;122:1218-23.

[25] Dicke RH. The effect of collisions upon the Doppler width of spectral lines. Phys Rev 1953;89:472-3.

[26] Ritter KJ, Wilkerson TD. High-resolution spectroscopy of the oxygen A-band. J Mol Spectrosc 1987;121:1-19.

[27] Robichaud DJ, Hodges JT, Brown LR, Lisak D, Maslowski P, Yeung LY, Okumura M, Miller CE. Experimental intensity and lineshape parameters of the oxygen A-band using frequency-stabilized cavity ring-down spectroscopy. J Mol Spectrosc 2008;248:1-13.

[28] Long DA, Havey DK, Okumura M, Miller CE, Hodges JT. Cavity ring-down spectroscopy measurements of sub-Doppler hyperfine structure. Phys Rev A 2010;81:064502.

[29] Robichaud DJ, Hodges JT, Lisak D, Miller CE, Okumura M. High-precision pressure shifting measurement technique using frequency-stabilized cavity ring-down spectroscopy. JQSRT 2008;109:435-44.
[30] Pickett HM. The fitting and prediction of vibration-rotation spectra with spin interactions. J Mol Spectrosc 1991;148:371-7.
[31] Rouillé G, Millot G, Saintloup R, Berger H. High-resolution stimulated Raman-spectroscopy of O_2. J Mol Spectrosc 1992;154:372-82.
[32] Cazzoli G, Esposti CD, Favero PG, Severi G. Microwave Spectra of $^{16}O^{17}O$ and $^{18}O^{17}O$. Nuovo Cimento B 1981;62:243-54.
[33] Mizushima M, Yamamoto S. Microwave absorption lines of $^{16}O^{18}O$ in its $X^3\Sigma_g^-$ (v=0) state. J Mol Spectrosc 1991;148:447-52.
[34] Amano T, Hirota E. Microwave spectrum of the molecular oxygen in the excited vibrational state. J Mol Spectrosc 1974;53:346-63.
[35] Steinbach W, Gordy W. Microwave spectrum and molecular constants of $^{16}O^{18}O$. Phys Rev A 1975;11:729-31.
[36] Endo Y, Mizushima M. Microwave absorption lines of $^{18}O_2$ in its electronic ground state ($X^3\Sigma_g^-$). Jpn J Appl Phys, Part 2 1983;22:L534-L6.
[37] Cazzoli G, Esposti CD, Landsberg BM. Millimeter wave spectrum of $^{17}O_2$ - magnetic hyperfine structure and quadrupole coupling constants. Nuovo Cimento D 1984;3:341-60.
[38] Steinbach W, Gordy W. Millimeter and submillimeter wave spectrum of $^{18}O_2$. Phys Rev A 1973;8:1753-8.
[39] Crownover RL, Delucia FC, Herbst E. The submillimeter-wave spectrum of $^{16}O^{18}O$. Astrophys J 1990;349:L29-L31.
[40] Drouin BJ, Yu SS, Miller CE, Muller HSP, Lewen F, Bruenken S, Habara H. Terahertz spectroscopy of oxygen, O_2, in its $^3\Sigma_g^-$and $^1\Delta$ electronic states: THz spectroscopy of O_2. JQSRT 2010;111:1167-73.
[41] Edwards HGM, Good EAM, Long DA. Pure rotational Raman spectra of $^{16}O_2$, $^{16}O^{18}O$, and $^{18}O_2$. J Chem Soc, Faraday Trans 2 1976;72:865-70.
[42] Jacquinet-Husson N, Scott NA, Chedina A, Crepeau L, Armante R, Capelle V, Orphal J, Coustenis A, Boonne C, Poulet-Crovisier N, Barbee A, Birk M, Brown LR, Camy-Peyret C, Claveau C, Chance K, Christidis N, Clerbaux C, Coheur PF, Dana V, Daumont L, De Backer-Barilly MR, Di Lonardo G, Flaud JM, Goldman A, Hamdouni A, Hess M, Hurley MD, Jacquemart D, Kleiner I, Kopke P, Mandin JY, Massie S, Mikhailenko S, Nemtchinov V, Nikitin A, Newnham D, Perrin A, Perevalov VI, Pinnock S, Regalia-Jarlot L, Rinsland CP, Rublev A, Schreier F, Schult L, Smith KM, Tashkun SA, Teffo JL, Toth RA, Tyuterev VG, Auwera JV, Varanasi P, Wagner G. The GEISA spectroscopic database: Current and future archive for Earth and planetary atmosphere studies. JQSRT 2008;109:1043-59.
[43] Herman R, Wallis RF. Influence of vibration-rotation interaction on line intensities in vibration-rotation bands of diatomic molecules. J Chem Phys 1955;23:637-46.
[44] Watson JKG. Quadratic Herman-Wallis factors in the fundamental bands of linear molecules. J Mol Spectrosc 1987;125:428-41.
[45] Schermaul R, Learner RCM. Precise line parameters and transition probability of the atmospheric A band of molecular oxygen $^{16}O_2$. JQSRT 1999;61:781-94.

[46] Brown LR, Plymate C. Experimental line parameters of the oxygen A band at 760 nm. J Mol Spectrosc 2000;199:166-79.
[47] Gamache RR, Goldman A, Rothman LS. Improved spectral parameters for the three most abundant isotopomers of the oxygen molecule. JQSRT 1998;59:495-509.
[48] Watson JKG. Rotational line intensities in $^3\Sigma$-$^1\Sigma$ electronic transitions. Can J Phys 1968;46:1637-43.
[49] Chackerian C, Tipping RH. Vibration-rotational and rotational intensities for CO isotopes. J Mol Spectrosc 1983;99:431-49.
[50] Singh SJ. Infrared band intensities: transition-moment matrix elements for fundamental and overtone bands; III isotope effects. J Mol Struct 1985;127:203-8.
[51] Long DA, Havey DK, Okumura M, Pickett HM, Miller CE, Hodges JT. Laboratory measurements and theoretical calculations of O_2 A-band electric quadrupole transitions. Phys Rev A 2009;80:042513.

Table 1: Composition of Isotopically Enriched Samples

Iso.	Natural Abundance[a]	^{18}O-Enriched Sample[b]	^{17}O-Enriched Sample[c]	Calculated Band Intensity[d] (cm molec.$^{-1}$)	Measured Band Intensity[e] (cm molec.$^{-1}$)
$^{16}O_2$	0.995262	0.2784 (51)	0.1523	2.231E-22	2.231(7)E-22
$^{16}O^{17}O$	0.000742	0.0099 (4)	0.3816	1.663E-25	1.77(7)E-25
$^{16}O^{18}O$	0.00399141	0.3672 (18)	0.0828	8.947E-25	9.13(5)E-25
$^{17}O_2$	1.38×10^{-7}	not determined	0.2593	3.093E-29	not determined
$^{17}O^{18}O$	1.49×10^{-6}	0.0174 (4)	0.1115	3.340E-28	3.37(8)E-28
$^{18}O_2$	4.00178×10^{-6}	0.3271 (32)	0.0125	8.970E-28	8.66(9)E-28

[a]Based upon the HITRAN 2004 recommended values [17]. [b]Composition determined by mass spectrometer. Values in parentheses are standard uncertainties (1σ). Note that $^{16}O^{18}O$ abundance is actually $^{16}O^{18}O + {}^{17}O_2$ (i.e. mass 34). The uncertainty due to this assumption should be less than 0.01%. [c]Supplier provided composition data. [d]Band intensities at T_{ref}=296 K and natural terrestrial abundance as determined by scaling the FS-CRDS determined $^{16}O_2$ band intensity by the natural abundance [17]. [e]Band intensities at T_{ref}=296 K and natural terrestrial isotopic abundance as determined by a fit to the FS-CRDS rare isotopologue measurements. This fit employed the Gamache et al. intensity model [47] with the Hönl-London factors of Watson [48] and a quadratic Herman-Wallis-like correction [44] as described in the text.

Table 2. Lower state ($X^3\Sigma_g^-$) molecular constants determined through the described global fit for each of the O_2 isotopologues (Iso.). All values are in cm^{-1}. Lower state energy levels are defined by Rouillé et al. [31]. Values in parentheses are standard uncertainties in the final digit. $^{16}O_2$ parameters were determined through a global fit as described in Long et al. [51].

Iso.	B_0	D_0 (10^{-6})	H_0 (10^{-12})	λ_0	λ_0' (10^{-6})	λ_0'' (10^{-12})	μ_0 (10^{-3})	μ_0' (10^{-9})	μ_0'' (10^{-14})
1616	1.437676078(29)	4.84178(14)	4.28(19)	1.98475118(5)	1.9470(3)	9.70(3)	-8.4253696(58)	-8.136(22)	-4.04(15)
1617	1.3953309(28)	4.541(12)		1.98471099(30)	1.8887(38)		-8.176541(78)	-7.13(59)	
1618	1.357852204(61)	4.3141(22)	-28(22)	1.98467434(16)	1.83330(86)	9.57(81)	-7.956002(11)	-7.275(39)	
1717	1.3529812(23)	3.9(10)		1.98466937(57)	1.82776(88)		-7.9278(11)	-7.194(90)	
1718	1.3154968(23)	4.0485(84)		1.98463263(69)	1.7847(96)		-7.70718(12)	-7.0(1)	
1818	1.278008487(57)	3.82340(42)	3.8(11)	1.984595545(42)	1.72139(23)	7.73(24)	-7.4866992(46)	-6.418(16)	-3.8(1)

Table 3. Upper state ($b^1\Sigma_g^+$) molecular constants determined through the described global fit for each of the O_2 isotopologues (Iso.). All values are in cm^{-1}. Upper state energy levels are given by $T+BJ(J+1)-DJ^2(J+1)^2+HJ^3(J+1)^3$. Values in parentheses are standard uncertainties in the final digit. $^{16}O_2$ parameters were determined through a global fit as described in Long et al. [51].

Iso.	T	B	D (10^{-6})	H (10^{-12})
1616	13122.0057456(89)	1.39124922(11)	5.36909(28)	0.0165(33)
1617	13123.803741(92)	1.3502891(32)	5.028(31)	
1618	13124.793138(23)	1.31404418(43)	4.7858(18)	-36(25)
1717	13124.92252(26)	1.309331(24)	4.43(88)	
1718	13125.92895(11)	1.2730753(29)	4.487(11)	
1818	13126.516194(33)	1.27800849(41)	4.2381(13)	

Table 4. Line parameters of $b^1\Sigma_g^+ \leftarrow X^3\Sigma_g^-(0,0)$ magnetic dipole transitions for $^{16}O^{18}O$ (1618). Transition frequencies ($\tilde{\nu}$) and lower state energies (E'') were calculated using the molecular parameters determined during the global fit (see Tables 2 and 3) and the formalism of Rouillé et al. [31]. Line intensities (S) at T_{ref}=296 K and natural terrestrial isotopic abundance [17] were calculated using the standard model of Gamache et al. [47] with the Hönl-London factors (L, also calculated with the molecular parameters of Tables 2 and 3) of Watson [48] and a band intensity S_b=8.947×10^{-25} cm molec.$^{-1}$. These intensities included a quadratic Herman-Wallis-like correction [44], given by $(1+a_1m+a_2m^2)^2$ where a_1= –2.6580×10^{-4} and a_2= 3.3622×10^{-6}. Einstein-A coefficients were calculated based upon these intensities as described in the text. Note 1 cm^{-1} atm^{-1} = 0.295872 MHz Pa^{-1}. Uncertainties are comparable to those given in Table 4 of Robichaud et al. [15].

Transition	L	$\tilde{\nu}$ (cm^{-1})	S (cm molec.$^{-1}$)	A (s^{-1})	E'' (cm^{-1})	γ_{air} (MHz Pa^{-1})	γ_{self} (MHz Pa^{-1})	δ (MHz Pa^{-1})	η_{air} (MHz Pa^{-1})	η_{self} (MHz Pa^{-1})
P41Q40	20.3643	12941.361526	1.487E-30	0.02142	2325.43140	7.29E-03	8.48E-03	-3.02E-03	5.93E-03	5.15E-03
P40P40	20.5000	12945.953401	2.538E-30	0.02213	2216.96355	7.41E-03	8.59E-03	-3.00E-03	6.34E-03	5.11E-03
P40Q39	19.8643	12947.629006	2.478E-30	0.02143	2215.28795	7.41E-03	8.59E-03	-3.00E-03	5.89E-03	5.11E-03
P39P39	20.0000	12952.120128	4.174E-30	0.02216	2109.45667	7.55E-03	8.72E-03	-2.98E-03	6.28E-03	5.07E-03
P39Q38	19.3643	12953.803756	4.071E-30	0.02144	2107.77304	7.55E-03	8.72E-03	-2.98E-03	5.84E-03	5.07E-03
P38P38	19.5000	12958.194499	6.772E-30	0.02219	2004.58270	7.70E-03	8.85E-03	-2.96E-03	6.22E-03	5.02E-03
P38Q37	18.8643	12959.886163	6.599E-30	0.02145	2002.89103	7.70E-03	8.85E-03	-2.96E-03	5.79E-03	5.02E-03
P37P37	19.0000	12964.176885	1.084E-29	0.02222	1902.34587	7.86E-03	9.00E-03	-2.94E-03	6.15E-03	4.96E-03
P37Q36	18.3643	12965.876597	1.055E-29	0.02146	1900.64616	7.86E-03	9.00E-03	-2.94E-03	5.73E-03	4.96E-03
P36P36	18.5000	12970.067641	1.711E-29	0.02225	1802.75031	8.04E-03	9.15E-03	-2.91E-03	6.08E-03	4.91E-03
P36Q35	17.8643	12971.775414	1.665E-29	0.02147	1801.04253	8.04E-03	9.15E-03	-2.91E-03	5.66E-03	4.91E-03
P35P35	18.0000	12975.867106	2.666E-29	0.02228	1705.80000	8.24E-03	9.32E-03	-2.89E-03	6.00E-03	4.84E-03
P35Q34	17.3643	12977.582955	2.591E-29	0.02148	1704.08415	8.24E-03	9.32E-03	-2.89E-03	5.59E-03	4.84E-03
P34P34	17.5000	12981.575607	4.098E-29	0.02232	1611.49884	8.46E-03	9.50E-03	-2.87E-03	5.91E-03	4.78E-03
P34Q33	16.8643	12983.299546	3.979E-29	0.02149	1609.77490	8.46E-03	9.50E-03	-2.87E-03	5.52E-03	4.78E-03
P33P33	17.0000	12987.193454	6.211E-29	0.02236	1519.85059	8.70E-03	9.69E-03	-2.84E-03	5.81E-03	4.71E-03
P33Q32	16.3644	12988.925501	6.024E-29	0.02151	1518.11854	8.70E-03	9.69E-03	-2.84E-03	5.44E-03	4.71E-03
P32P32	16.5000	12992.720944	9.286E-29	0.02240	1430.85890	8.96E-03	9.89E-03	-2.82E-03	5.71E-03	4.63E-03
P32Q31	15.8644	12994.461116	8.997E-29	0.02152	1429.11872	8.96E-03	9.89E-03	-2.82E-03	5.35E-03	4.63E-03
P31P31	16.0000	12998.158360	1.369E-28	0.02243	1344.52730	9.23E-03	1.01E-02	-2.79E-03	5.60E-03	4.55E-03
P31Q30	15.3644	12999.906677	1.325E-28	0.02153	1342.77898	9.23E-03	1.01E-02	-2.79E-03	5.25E-03	4.55E-03
P30P30	15.5000	13003.505971	1.991E-28	0.02248	1260.85922	9.52E-03	1.03E-02	-2.77E-03	5.48E-03	4.47E-03
P30Q29	14.8644	13005.262455	1.924E-28	0.02154	1259.10274	9.52E-03	1.03E-02	-2.77E-03	5.15E-03	4.47E-03
P29P29	15.0000	13008.764033	2.856E-28	0.02252	1179.85797	9.83E-03	1.05E-02	-2.74E-03	5.36E-03	4.39E-03
P29Q28	14.3644	13010.528707	2.756E-28	0.02156	1178.09330	9.83E-03	1.05E-02	-2.74E-03	5.04E-03	4.39E-03
P28P28	14.5000	13013.932787	4.036E-28	0.02257	1101.52674	1.01E-02	1.08E-02	-2.71E-03	5.23E-03	4.30E-03
P28Q27	13.8644	13015.705676	3.890E-28	0.02157	1099.75385	1.01E-02	1.08E-02	-2.71E-03	4.93E-03	4.30E-03
P27P27	14.0000	13019.012462	5.627E-28	0.02262	1025.86861	1.05E-02	1.10E-02	-2.69E-03	5.10E-03	4.21E-03
P27Q26	13.3644	13020.793595	5.414E-28	0.02158	1024.08748	1.05E-02	1.10E-02	-2.69E-03	4.82E-03	4.21E-03
P26P26	13.5000	13024.003273	7.733E-28	0.02268	952.88657	1.08E-02	1.12E-02	-2.66E-03	4.96E-03	4.13E-03
P26Q25	12.8644	13025.792682	7.428E-28	0.02160	951.09716	1.08E-02	1.12E-02	-2.66E-03	4.70E-03	4.13E-03
P25P25	13.0000	13028.905423	1.047E-27	0.02273	882.58346	1.11E-02	1.15E-02	-2.63E-03	4.83E-03	4.04E-03
P25Q24	12.3644	13030.703143	1.004E-27	0.02161	880.78574	1.11E-02	1.15E-02	-2.63E-03	4.59E-03	4.04E-03
P24P24	12.5000	13033.719101	1.398E-27	0.02279	814.96204	1.15E-02	1.17E-02	-2.60E-03	4.70E-03	3.96E-03
P24Q23	11.8644	13035.525171	1.338E-27	0.02163	813.15597	1.15E-02	1.17E-02	-2.60E-03	4.47E-03	3.96E-03
P23P23	12.0000	13038.444484	1.840E-27	0.02286	750.02495	1.18E-02	1.19E-02	-2.57E-03	4.57E-03	3.88E-03
P23Q22	11.3644	13040.258949	1.756E-27	0.02164	748.21048	1.18E-02	1.19E-02	-2.57E-03	4.36E-03	3.88E-03

P22P22	11.5000	13043.081737	2.385E-27	0.02293	687.77471	1.21E-02	1.21E-02	-2.54E-03	4.45E-03	3.80E-03
P22Q21	10.8644	13044.904646	2.271E-27	0.02166	685.95181	1.21E-02	1.21E-02	-2.54E-03	4.26E-03	3.80E-03
P21P21	11.0000	13047.631011	3.046E-27	0.02301	628.21376	1.23E-02	1.23E-02	-2.50E-03	4.34E-03	3.72E-03
P21Q20	10.3644	13049.462421	2.894E-27	0.02168	626.38235	1.23E-02	1.23E-02	-2.50E-03	4.16E-03	3.72E-03
P20P20	10.5000	13052.092445	3.832E-27	0.02310	571.34441	1.26E-02	1.25E-02	-2.47E-03	4.23E-03	3.65E-03
P20Q19	9.8644	13053.932422	3.630E-27	0.02169	569.50443	1.26E-02	1.25E-02	-2.47E-03	4.07E-03	3.65E-03
P19P19	10.0000	13056.466167	4.746E-27	0.02319	517.16885	1.28E-02	1.27E-02	-2.44E-03	4.14E-03	3.59E-03
P19Q18	9.3644	13058.314787	4.482E-27	0.02170	515.32023	1.28E-02	1.27E-02	-2.44E-03	3.99E-03	3.59E-03
P18P18	9.5000	13060.752291	5.789E-27	0.02329	465.68920	1.30E-02	1.29E-02	-2.40E-03	4.05E-03	3.52E-03
P18Q17	8.8644	13062.609642	5.447E-27	0.02172	463.83185	1.30E-02	1.29E-02	-2.40E-03	3.92E-03	3.52E-03
P17P17	9.0000	13064.950922	6.949E-27	0.02341	416.90743	1.32E-02	1.30E-02	-2.37E-03	3.98E-03	3.47E-03
P17Q16	8.3644	13066.817107	6.512E-27	0.02175	415.04124	1.32E-02	1.30E-02	-2.37E-03	3.85E-03	3.47E-03
P16P16	8.5000	13069.062149	8.206E-27	0.02354	370.82543	1.34E-02	1.32E-02	-2.33E-03	3.91E-03	3.41E-03
P16Q15	7.8644	13070.937292	7.658E-27	0.02177	368.95028	1.34E-02	1.32E-02	-2.33E-03	3.79E-03	3.41E-03
P15P15	8.0000	13073.086052	9.532E-27	0.02368	327.44497	1.36E-02	1.33E-02	-2.30E-03	3.85E-03	3.35E-03
P15Q14	7.3644	13074.970302	8.851E-27	0.02180	325.56072	1.36E-02	1.33E-02	-2.30E-03	3.74E-03	3.35E-03
P14P14	7.5000	13077.022698	1.089E-26	0.02386	286.76774	1.37E-02	1.35E-02	-2.26E-03	3.79E-03	3.30E-03
P14Q13	6.8644	13078.916235	1.005E-26	0.02183	284.87420	1.37E-02	1.35E-02	-2.26E-03	3.69E-03	3.30E-03
P13P13	7.0000	13080.872144	1.221E-26	0.02405	248.79528	1.39E-02	1.36E-02	-2.22E-03	3.73E-03	3.25E-03
P13Q12	6.3644	13082.775192	1.120E-26	0.02186	246.89223	1.39E-02	1.36E-02	-2.22E-03	3.64E-03	3.25E-03
P12P12	6.5000	13084.634433	1.346E-26	0.02428	213.52906	1.40E-02	1.38E-02	-2.18E-03	3.67E-03	3.19E-03
P12Q11	5.8644	13086.547273	1.225E-26	0.02190	211.61622	1.40E-02	1.38E-02	-2.18E-03	3.59E-03	3.19E-03
P11P11	6.0000	13088.309598	1.455E-26	0.02455	180.97044	1.42E-02	1.39E-02	-2.15E-03	3.61E-03	3.13E-03
P11Q10	5.3644	13090.232590	1.312E-26	0.02194	179.04745	1.42E-02	1.39E-02	-2.15E-03	3.53E-03	3.13E-03
P10P10	5.5000	13091.897660	1.541E-26	0.02488	151.12066	1.43E-02	1.41E-02	-2.11E-03	3.54E-03	3.06E-03
P10Q9	4.8645	13093.831279	1.375E-26	0.02200	149.18704	1.43E-02	1.41E-02	-2.11E-03	3.47E-03	3.06E-03
P9P9	5.0000	13095.398629	1.598E-26	0.02528	123.98087	1.45E-02	1.43E-02	-2.07E-03	3.46E-03	2.99E-03
P9Q8	4.3645	13097.343514	1.408E-26	0.02206	122.03598	1.45E-02	1.43E-02	-2.07E-03	3.41E-03	2.99E-03
P8P8	4.5000	13098.812502	1.619E-26	0.02579	99.55209	1.47E-02	1.45E-02	-2.02E-03	3.37E-03	2.91E-03
P8Q7	3.8645	13100.769551	1.403E-26	0.02215	97.59505	1.47E-02	1.45E-02	-2.02E-03	3.33E-03	2.91E-03
P7P7	4.0000	13102.139268	1.599E-26	0.02645	77.83528	1.50E-02	1.47E-02	-1.98E-03	3.27E-03	2.82E-03
P7Q6	3.3646	13104.109789	1.357E-26	0.02225	75.86476	1.50E-02	1.47E-02	-1.98E-03	3.24E-03	2.82E-03
P6P6	3.5000	13105.378901	1.533E-26	0.02736	58.83125	1.53E-02	1.50E-02	-1.94E-03	3.14E-03	2.72E-03
P6Q5	2.8647	13107.364921	1.266E-26	0.02239	56.84523	1.53E-02	1.50E-02	-1.94E-03	3.13E-03	2.72E-03
P5P5	3.0000	13108.531365	1.422E-26	0.02867	42.54074	1.57E-02	1.53E-02	-1.90E-03	2.99E-03	2.60E-03
P5Q4	2.3649	13110.536270	1.132E-26	0.02260	40.53584	1.57E-02	1.53E-02	-1.90E-03	3.00E-03	2.60E-03
P4P4	2.5000	13111.596614	1.265E-26	0.03072	28.96436	1.61E-02	1.57E-02	-1.85E-03	2.81E-03	2.46E-03
P4Q3	1.8653	13113.626722	9.532E-27	0.02292	26.93426	1.61E-02	1.57E-02	-1.85E-03	2.85E-03	2.46E-03
P3P3	2.0000	13114.574588	1.066E-26	0.03441	18.10264	1.67E-02	1.62E-02	-1.81E-03	2.59E-03	2.29E-03
P3Q2	1.3662	13116.643966	7.359E-27	0.02350	16.03326	1.67E-02	1.62E-02	-1.81E-03	2.66E-03	2.29E-03
P2P2	1.5000	13117.465220	8.323E-27	0.04302	9.95599	1.73E-02	1.67E-02	-1.77E-03	2.32E-03	2.08E-03
P2Q1	0.8697	13119.617605	4.874E-27	0.02494	7.80360	1.73E-02	1.67E-02	-1.77E-03	2.42E-03	2.08E-03
P1P1	1.0000	13120.268426	5.695E-27	0.08603	4.52471	1.82E-02	1.74E-02	-1.72E-03	1.97E-03	1.84E-03
R0Q1	0.6303	13127.421207	3.665E-27	0.01807	0.00000	1.73E-02	1.67E-02	-1.77E-03	4.25E-03	2.08E-03
R1R1	0.5000	13128.152519	2.845E-27	0.00861	4.52471	1.67E-02	1.62E-02	-1.81E-03	4.29E-03	2.29E-03
R1Q2	1.1338	13130.044563	6.508E-27	0.01951	2.63267	1.67E-02	1.62E-02	-1.81E-03	4.28E-03	2.29E-03
R2R2	1.0000	13130.604991	5.539E-27	0.01230	9.95599	1.61E-02	1.57E-02	-1.85E-03	4.33E-03	2.46E-03
R2Q3	1.6347	13132.536326	9.137E-27	0.02010	8.02465	1.61E-02	1.57E-02	-1.85E-03	4.31E-03	2.46E-03
R3R3	1.5000	13132.969465	7.984E-27	0.01434	18.10264	1.57E-02	1.53E-02	-1.90E-03	4.37E-03	2.60E-03
R3Q4	2.1351	13134.926032	1.147E-26	0.02042	16.14607	1.57E-02	1.53E-02	-1.90E-03	4.34E-03	2.60E-03

R4R4	2.0000	13135.245790	1.010E-26	0.01565	28.96436	1.53E-02	1.50E-02	-1.94E-03	4.40E-03	2.72E-03
R4Q5	2.6353	13137.221279	1.342E-26	0.02062	26.98888	1.53E-02	1.50E-02	-1.94E-03	4.36E-03	2.72E-03
R5R5	2.5000	13137.433807	1.181E-26	0.01655	42.54074	1.50E-02	1.47E-02	-1.98E-03	4.43E-03	2.82E-03
R5Q6	3.1354	13139.424838	1.495E-26	0.02076	40.54971	1.50E-02	1.47E-02	-1.98E-03	4.37E-03	2.82E-03
R6R6	3.0000	13139.533343	1.309E-26	0.01722	58.83125	1.47E-02	1.45E-02	-2.02E-03	4.45E-03	2.91E-03
R6Q7	3.6355	13141.537898	1.601E-26	0.02086	56.82670	1.47E-02	1.45E-02	-2.02E-03	4.39E-03	2.91E-03
R7R7	3.5000	13141.544215	1.392E-26	0.01772	77.83528	1.45E-02	1.43E-02	-2.07E-03	4.46E-03	2.99E-03
R7Q8	4.1355	13143.560991	1.660E-26	0.02094	75.81850	1.45E-02	1.43E-02	-2.07E-03	4.40E-03	2.99E-03
R8R8	4.0000	13143.466228	1.431E-26	0.01812	99.55209	1.43E-02	1.41E-02	-2.11E-03	4.48E-03	3.06E-03
R8Q9	4.6355	13145.494336	1.675E-26	0.02100	97.52399	1.43E-02	1.41E-02	-2.11E-03	4.41E-03	3.06E-03
R9R9	4.5000	13145.299174	1.429E-26	0.01845	123.98087	1.42E-02	1.39E-02	-2.15E-03	4.49E-03	3.13E-03
R9Q10	5.1356	13147.337981	1.647E-26	0.02105	121.94206	1.42E-02	1.39E-02	-2.15E-03	4.42E-03	3.13E-03
R10R10	5.0000	13147.042835	1.391E-26	0.01872	151.12066	1.40E-02	1.38E-02	-2.18E-03	4.51E-03	3.19E-03
R10Q11	5.6356	13149.091875	1.583E-26	0.02109	149.07162	1.40E-02	1.38E-02	-2.18E-03	4.43E-03	3.19E-03
R11R11	5.5000	13148.696981	1.323E-26	0.01894	180.97044	1.39E-02	1.36E-02	-2.22E-03	4.52E-03	3.25E-03
R11Q12	6.1356	13150.755900	1.491E-26	0.02113	178.91152	1.39E-02	1.36E-02	-2.22E-03	4.44E-03	3.25E-03
R12R12	6.0000	13150.261369	1.232E-26	0.01913	213.52906	1.37E-02	1.35E-02	-2.26E-03	4.53E-03	3.30E-03
R12Q13	6.6356	13152.329893	1.376E-26	0.02116	211.46054	1.37E-02	1.35E-02	-2.26E-03	4.44E-03	3.30E-03
R13R13	6.5000	13151.735743	1.124E-26	0.01929	248.79528	1.36E-02	1.33E-02	-2.30E-03	4.54E-03	3.35E-03
R13Q14	7.1356	13153.813656	1.246E-26	0.02119	246.71737	1.36E-02	1.33E-02	-2.30E-03	4.45E-03	3.35E-03
R14R14	7.0000	13153.119839	1.007E-26	0.01944	286.76774	1.34E-02	1.32E-02	-2.33E-03	4.56E-03	3.41E-03
R14Q15	7.6356	13155.206967	1.109E-26	0.02121	284.68061	1.34E-02	1.32E-02	-2.33E-03	4.46E-03	3.41E-03
R15R15	7.5000	13154.413376	8.847E-27	0.01956	327.44497	1.32E-02	1.30E-02	-2.37E-03	4.57E-03	3.47E-03
R15Q16	8.1356	13156.509579	9.695E-27	0.02122	325.34877	1.32E-02	1.30E-02	-2.37E-03	4.47E-03	3.47E-03
R16R16	8.0000	13155.616062	7.641E-27	0.01968	370.82543	1.30E-02	1.29E-02	-2.40E-03	4.59E-03	3.52E-03
R16Q17	8.6356	13157.721224	8.332E-27	0.02124	368.72026	1.30E-02	1.29E-02	-2.40E-03	4.48E-03	3.52E-03
R17R17	8.5000	13156.727595	6.488E-27	0.01977	416.90743	1.28E-02	1.27E-02	-2.44E-03	4.60E-03	3.59E-03
R17Q18	9.1356	13158.841619	7.045E-27	0.02125	414.79340	1.28E-02	1.27E-02	-2.44E-03	4.49E-03	3.59E-03
R18R18	9.0000	13157.747658	5.418E-27	0.01986	465.68920	1.26E-02	1.25E-02	-2.47E-03	4.62E-03	3.65E-03
R18Q19	9.6356	13159.870463	5.861E-27	0.02127	463.56639	1.26E-02	1.25E-02	-2.47E-03	4.50E-03	3.65E-03
R19R19	9.5000	13158.675921	4.452E-27	0.01994	517.16885	1.23E-02	1.23E-02	-2.50E-03	4.64E-03	3.72E-03
R19Q20	10.1356	13160.807439	4.799E-27	0.02128	515.03734	1.23E-02	1.23E-02	-2.50E-03	4.52E-03	3.72E-03
R20R20	10.0000	13159.512042	3.601E-27	0.02001	571.34441	1.21E-02	1.21E-02	-2.54E-03	4.67E-03	3.80E-03
R20Q21	10.6356	13161.652214	3.869E-27	0.02129	569.20424	1.21E-02	1.21E-02	-2.54E-03	4.53E-03	3.80E-03
R21R21	10.5000	13160.255666	2.867E-27	0.02008	628.21376	1.18E-02	1.19E-02	-2.57E-03	4.69E-03	3.88E-03
R21Q22	11.1356	13162.404443	3.073E-27	0.02130	626.06499	1.18E-02	1.19E-02	-2.57E-03	4.55E-03	3.88E-03
R22R22	11.0000	13160.906424	2.248E-27	0.02014	687.77471	1.15E-02	1.17E-02	-2.60E-03	4.72E-03	3.96E-03
R22Q23	11.6356	13163.063763	2.403E-27	0.02131	685.61737	1.15E-02	1.17E-02	-2.60E-03	4.56E-03	3.96E-03
R23R23	11.5000	13161.463934	1.736E-27	0.02019	750.02495	1.11E-02	1.15E-02	-2.63E-03	4.74E-03	4.04E-03
R23Q24	12.1356	13163.629799	1.851E-27	0.02131	747.85908	1.11E-02	1.15E-02	-2.63E-03	4.58E-03	4.04E-03
R24R24	12.0000	13161.927802	1.321E-27	0.02024	814.96204	1.08E-02	1.12E-02	-2.66E-03	4.77E-03	4.13E-03
R24Q25	12.6356	13164.102161	1.406E-27	0.02132	812.78768	1.08E-02	1.12E-02	-2.66E-03	4.60E-03	4.13E-03
R25R25	12.5000	13162.297618	9.906E-28	0.02028	882.58346	1.05E-02	1.10E-02	-2.69E-03	4.80E-03	4.21E-03
R25Q26	13.1356	13164.480442	1.052E-27	0.02132	880.40063	1.05E-02	1.10E-02	-2.69E-03	4.62E-03	4.21E-03
R26R26	13.0000	13162.572959	7.319E-28	0.02033	952.88657	1.01E-02	1.08E-02	-2.71E-03	4.82E-03	4.30E-03
R26Q27	13.6356	13164.764225	7.759E-28	0.02133	950.69530	1.01E-02	1.08E-02	-2.71E-03	4.63E-03	4.30E-03
R27R27	13.5000	13162.753388	5.331E-28	0.02037	1025.86861	9.83E-03	1.05E-02	-2.74E-03	4.85E-03	4.39E-03
R27Q28	14.1356	13164.953075	5.641E-28	0.02133	1023.66893	9.83E-03	1.05E-02	-2.74E-03	4.65E-03	4.39E-03
R28R28	14.0000	13162.838454	3.826E-28	0.02040	1101.52674	9.52E-03	1.03E-02	-2.77E-03	4.87E-03	4.47E-03
R28Q29	14.6356	13165.046543	4.043E-28	0.02134	1099.31865	9.52E-03	1.03E-02	-2.77E-03	4.67E-03	4.47E-03

R29R29	14.5000	13162.827691	2.708E-28	0.02044	1179.85797	9.23E-03	1.01E-02	-2.79E-03	4.90E-03	4.55E-03
R29Q30	15.1356	13165.044166	2.857E-28	0.02134	1177.64149	9.23E-03	1.01E-02	-2.79E-03	4.68E-03	4.55E-03
R30R30	15.0000	13162.720619	1.889E-28	0.02047	1260.85922	8.96E-03	9.89E-03	-2.82E-03	4.92E-03	4.63E-03
R30Q31	15.6356	13164.945467	1.991E-28	0.02134	1258.63437	8.96E-03	9.89E-03	-2.82E-03	4.70E-03	4.63E-03
R31R31	15.5000	13162.516742	1.300E-28	0.02049	1344.52730	8.70E-03	9.69E-03	-2.84E-03	4.94E-03	4.71E-03
R31Q32	16.1356	13164.749950	1.368E-28	0.02134	1342.29409	8.70E-03	9.69E-03	-2.84E-03	4.71E-03	4.71E-03
R32R32	16.0000	13162.215551	8.817E-29	0.02052	1430.85890	8.46E-03	9.50E-03	-2.87E-03	4.96E-03	4.78E-03
R32Q33	16.6357	13164.457109	9.269E-29	0.02135	1428.61734	8.46E-03	9.50E-03	-2.87E-03	4.72E-03	4.78E-03
R33R33	16.5000	13161.816519	5.899E-29	0.02054	1519.85059	8.24E-03	9.32E-03	-2.89E-03	4.98E-03	4.84E-03
R33Q34	17.1357	13164.066417	6.194E-29	0.02135	1517.60069	8.24E-03	9.32E-03	-2.89E-03	4.74E-03	4.84E-03
R34R34	17.0000	13161.319105	3.892E-29	0.02057	1611.49884	8.04E-03	9.15E-03	-2.91E-03	5.00E-03	4.91E-03
R34Q35	17.6357	13163.577337	4.083E-29	0.02135	1609.24061	8.04E-03	9.15E-03	-2.91E-03	4.75E-03	4.91E-03
R35R35	17.5000	13160.722753	2.534E-29	0.02059	1705.80000	7.86E-03	9.00E-03	-2.94E-03	5.01E-03	4.96E-03
R35Q36	18.1357	13162.989311	2.655E-29	0.02135	1703.53344	7.86E-03	9.00E-03	-2.94E-03	4.76E-03	4.96E-03
R36R36	18.0000	13160.026890	1.627E-29	0.02061	1802.75031	7.70E-03	8.85E-03	-2.96E-03	5.02E-03	5.02E-03
R36Q37	18.6357	13162.301768	1.703E-29	0.02135	1800.47543	7.70E-03	8.85E-03	-2.96E-03	4.76E-03	5.02E-03
R37R37	18.5000	13159.230925	1.030E-29	0.02063	1902.34587	7.55E-03	8.72E-03	-2.98E-03	5.04E-03	5.07E-03
R37Q38	19.1357	13161.514119	1.077E-29	0.02135	1900.06268	7.55E-03	8.72E-03	-2.98E-03	4.77E-03	5.07E-03
R38R38	19.0000	13158.334255	6.435E-30	0.02064	2004.58270	7.41E-03	8.59E-03	-3.00E-03	5.05E-03	5.11E-03
R38Q39	19.6357	13160.625760	6.727E-30	0.02134	2002.29119	7.41E-03	8.59E-03	-3.00E-03	4.78E-03	5.11E-03
R39R39	19.5000	13157.336255	3.967E-30	0.02066	2109.45667	7.29E-03	8.48E-03	-3.02E-03	5.06E-03	5.15E-03
R39Q40	20.1357	13159.636069	4.143E-30	0.02134	2107.15685	7.29E-03	8.48E-03	-3.02E-03	4.79E-03	5.15E-03
R40R40	20.0000	13156.236287	2.413E-30	0.02068	2216.96355	7.17E-03	8.38E-03	-3.04E-03	5.07E-03	5.19E-03
R40Q41	20.6357	13158.544406	2.517E-30	0.02134	2214.65543	7.17E-03	8.38E-03	-3.04E-03	4.79E-03	5.19E-03

Table 5. Line parameters of $b^1\Sigma_g^+ \leftarrow X^3\Sigma_g^-(0,0)$ magnetic dipole transitions for $^{16}O^{17}O$ (1617). Transition frequencies ($\tilde{\nu}$) and lower state energies (E'') were calculated using the molecular parameters determined during the global fit (see Tables 2 and 3) and the formalism of Rouillé et al. [31]. Line intensities (S) at T_{ref}=296 K and natural terrestrial isotopic abundance [17] were calculated using the standard model of Gamache et al. [47] with the Hönl-London factors (L, also calculated with the molecular parameters of Tables 2 and 3) of Watson [48] and a band intensity S_b= 1.663×10^{-25} cm molec.$^{-1}$. These intensities included a quadratic Herman-Wallis-like correction [44], given by $(1+a_1m+a_2m^2)^2$ where a_1= -2.6580×10^{-4} and a_2= 3.3622×10^{-6}. Einstein-A coefficients were calculated based upon these intensities as described in the text. Note 1 cm^{-1} atm^{-1} = 0.295872 MHz Pa^{-1}. Uncertainties are comparable to those given in Table 6 of Robichaud et al. [15].

Transition	L	$\tilde{\nu}$ (cm^{-1})	S (cm molec.$^{-1}$)	A (s^{-1})	E'' (cm^{-1})	γ_{air} (MHz Pa^{-1})	γ_{self} (MHz Pa^{-1})	δ (MHz Pa^{-1})	η_{air} (MHz Pa^{-1})	η_{self} (MHz Pa^{-1})
P41Q40	20.3546	12935.320248	2.260E-31	0.02323	2389.43349	7.29E-03	8.48E-03	-3.02E-03	6.11E-03	5.31E-03
P40P40	20.5000	12940.090586	3.916E-31	0.02401	2277.92727	7.41E-03	8.59E-03	-3.00E-03	6.53E-03	5.27E-03
P40Q39	19.8546	12941.757977	3.820E-31	0.02324	2276.25988	7.41E-03	8.59E-03	-3.00E-03	6.06E-03	5.27E-03
P39P39	20.0000	12946.425220	6.532E-31	0.02405	2167.46318	7.55E-03	8.72E-03	-2.98E-03	6.47E-03	5.22E-03
P39Q38	19.3546	12948.100865	6.367E-31	0.02326	2165.78753	7.55E-03	8.72E-03	-2.98E-03	6.02E-03	5.22E-03
P38P38	19.5000	12952.665349	1.075E-30	0.02408	2059.70473	7.70E-03	8.85E-03	-2.96E-03	6.41E-03	5.17E-03
P38Q37	18.8546	12954.349261	1.047E-30	0.02327	2058.02082	7.70E-03	8.85E-03	-2.96E-03	5.96E-03	5.17E-03
P37P37	19.0000	12958.811310	1.744E-30	0.02412	1954.65617	7.86E-03	9.00E-03	-2.94E-03	6.34E-03	5.11E-03
P37Q36	18.3546	12960.503501	1.697E-30	0.02328	1952.96397	7.86E-03	9.00E-03	-2.94E-03	5.90E-03	5.11E-03
P36P36	18.5000	12964.863425	2.791E-30	0.02415	1852.32164	8.04E-03	9.15E-03	-2.91E-03	6.26E-03	5.05E-03
P36Q35	17.8546	12966.563910	2.713E-30	0.02330	1850.62115	8.04E-03	9.15E-03	-2.91E-03	5.84E-03	5.05E-03
P35P35	18.0000	12970.822007	4.404E-30	0.02419	1752.70517	8.24E-03	9.32E-03	-2.89E-03	6.18E-03	4.99E-03
P35Q34	17.3546	12972.530801	4.278E-30	0.02331	1750.99638	8.24E-03	9.32E-03	-2.89E-03	5.76E-03	4.99E-03
P34P34	17.5000	12976.687356	6.854E-30	0.02423	1655.81069	8.46E-03	9.50E-03	-2.87E-03	6.09E-03	4.92E-03
P34Q33	16.8546	12978.404475	6.651E-30	0.02332	1654.09357	8.46E-03	9.50E-03	-2.87E-03	5.69E-03	4.92E-03
P33P33	17.0000	12982.459761	1.052E-29	0.02427	1561.64201	8.70E-03	9.69E-03	-2.84E-03	5.99E-03	4.85E-03
P33Q32	16.3546	12984.185223	1.020E-29	0.02334	1559.91655	8.70E-03	9.69E-03	-2.84E-03	5.60E-03	4.85E-03
P32P32	16.5000	12988.139499	1.591E-29	0.02431	1470.20284	8.96E-03	9.89E-03	-2.82E-03	5.88E-03	4.77E-03
P32Q31	15.8546	12989.873323	1.541E-29	0.02335	1468.46902	8.96E-03	9.89E-03	-2.82E-03	5.51E-03	4.77E-03
P31P31	16.0000	12993.726835	2.374E-29	0.02436	1381.49677	9.23E-03	1.01E-02	-2.79E-03	5.77E-03	4.69E-03
P31Q30	15.3546	12995.469042	2.296E-29	0.02336	1379.75457	9.23E-03	1.01E-02	-2.79E-03	5.41E-03	4.69E-03
P30P30	15.5000	12999.222023	3.491E-29	0.02440	1295.52730	9.52E-03	1.03E-02	-2.77E-03	5.65E-03	4.61E-03
P30Q29	14.8546	13000.972635	3.371E-29	0.02338	1293.77668	9.52E-03	1.03E-02	-2.77E-03	5.30E-03	4.61E-03
P29P29	15.0000	13004.625304	5.060E-29	0.02445	1212.29779	9.83E-03	1.05E-02	-2.74E-03	5.52E-03	4.52E-03
P29Q28	14.3546	13006.384347	4.880E-29	0.02339	1210.53874	9.83E-03	1.05E-02	-2.74E-03	5.19E-03	4.52E-03
P28P28	14.5000	13009.936909	7.230E-29	0.02451	1131.81152	1.01E-02	1.08E-02	-2.71E-03	5.39E-03	4.43E-03
P28Q27	13.8546	13011.704410	6.962E-29	0.02340	1130.04402	1.01E-02	1.08E-02	-2.71E-03	5.08E-03	4.43E-03
P27P27	14.0000	13015.157057	1.018E-28	0.02456	1054.07165	1.05E-02	1.10E-02	-2.69E-03	5.25E-03	4.34E-03
P27Q26	13.3546	13016.933046	9.788E-29	0.02342	1052.29566	1.05E-02	1.10E-02	-2.69E-03	4.96E-03	4.34E-03
P26P26	13.5000	13020.285953	1.413E-28	0.02462	979.08123	1.08E-02	1.12E-02	-2.66E-03	5.11E-03	4.25E-03
P26Q25	12.8546	13022.070465	1.356E-28	0.02343	977.29672	1.08E-02	1.12E-02	-2.66E-03	4.84E-03	4.25E-03
P25P25	13.0000	13025.323794	1.932E-28	0.02468	906.84320	1.11E-02	1.15E-02	-2.63E-03	4.98E-03	4.16E-03
P25Q24	12.3546	13027.116866	1.851E-28	0.02345	905.05013	1.11E-02	1.15E-02	-2.63E-03	4.73E-03	4.16E-03
P24P24	12.5000	13030.270762	2.603E-28	0.02475	837.36040	1.15E-02	1.17E-02	-2.60E-03	4.84E-03	4.08E-03
P24Q23	11.8546	13032.072436	2.488E-28	0.02346	835.55873	1.15E-02	1.17E-02	-2.60E-03	4.61E-03	4.08E-03

P23P23	12.0000	13035.127030	3.454E-28	0.02482	770.63555	1.18E-02	1.19E-02	-2.57E-03	4.71E-03	3.99E-03
P23Q22	11.3546	13036.937353	3.295E-28	0.02348	768.82523	1.18E-02	1.19E-02	-2.57E-03	4.50E-03	3.99E-03
P22P22	11.5000	13039.892757	4.515E-28	0.02490	706.67127	1.21E-02	1.21E-02	-2.54E-03	4.59E-03	3.91E-03
P22Q21	10.8546	13041.711783	4.297E-28	0.02350	704.85225	1.21E-02	1.21E-02	-2.54E-03	4.39E-03	3.91E-03
P21P21	11.0000	13044.568092	5.812E-28	0.02499	645.47007	1.23E-02	1.23E-02	-2.50E-03	4.47E-03	3.84E-03
P21Q20	10.3546	13046.395881	5.517E-28	0.02351	643.64228	1.23E-02	1.23E-02	-2.50E-03	4.29E-03	3.84E-03
P20P20	10.5000	13049.153171	7.367E-28	0.02508	587.03433	1.26E-02	1.25E-02	-2.47E-03	4.36E-03	3.76E-03
P20Q19	9.8546	13050.989794	6.972E-28	0.02353	585.19771	1.26E-02	1.25E-02	-2.47E-03	4.20E-03	3.76E-03
P19P19	10.0000	13053.648120	9.193E-28	0.02519	531.36635	1.28E-02	1.27E-02	-2.44E-03	4.27E-03	3.70E-03
P19Q18	9.3546	13055.493658	8.671E-28	0.02355	529.52081	1.28E-02	1.27E-02	-2.44E-03	4.11E-03	3.70E-03
P18P18	9.5000	13058.053050	1.129E-27	0.02530	478.46832	1.30E-02	1.29E-02	-2.40E-03	4.18E-03	3.63E-03
P18Q17	8.8546	13059.907598	1.061E-27	0.02357	476.61377	1.30E-02	1.29E-02	-2.40E-03	4.04E-03	3.63E-03
P17P17	9.0000	13062.368065	1.364E-27	0.02543	428.34229	1.32E-02	1.30E-02	-2.37E-03	4.10E-03	3.57E-03
P17Q16	8.3546	13064.231733	1.277E-27	0.02360	426.47862	1.32E-02	1.30E-02	-2.37E-03	3.97E-03	3.57E-03
P16P16	8.5000	13066.593254	1.621E-27	0.02557	380.99023	1.34E-02	1.32E-02	-2.33E-03	4.03E-03	3.51E-03
P16Q15	7.8546	13068.466175	1.511E-27	0.02362	379.11731	1.34E-02	1.32E-02	-2.33E-03	3.91E-03	3.51E-03
P15P15	8.0000	13070.728695	1.894E-27	0.02573	336.41400	1.36E-02	1.33E-02	-2.30E-03	3.96E-03	3.46E-03
P15Q14	7.3546	13072.611027	1.756E-27	0.02365	334.53167	1.36E-02	1.33E-02	-2.30E-03	3.85E-03	3.46E-03
P14P14	7.5000	13074.774454	2.174E-27	0.02591	294.61534	1.37E-02	1.35E-02	-2.26E-03	3.90E-03	3.40E-03
P14Q13	6.8546	13076.666392	2.005E-27	0.02368	292.72340	1.37E-02	1.35E-02	-2.26E-03	3.80E-03	3.40E-03
P13P13	7.0000	13078.730587	2.452E-27	0.02613	255.59588	1.39E-02	1.36E-02	-2.22E-03	3.84E-03	3.34E-03
P13Q12	6.3546	13080.632369	2.246E-27	0.02371	253.69410	1.39E-02	1.36E-02	-2.22E-03	3.75E-03	3.34E-03
P12P12	6.5000	13082.597136	2.715E-27	0.02637	219.35715	1.40E-02	1.38E-02	-2.18E-03	3.78E-03	3.29E-03
P12Q11	5.8546	13084.509064	2.467E-27	0.02375	217.44522	1.40E-02	1.38E-02	-2.18E-03	3.69E-03	3.29E-03
P11P11	6.0000	13086.374132	2.947E-27	0.02667	185.90056	1.42E-02	1.39E-02	-2.15E-03	3.72E-03	3.22E-03
P11Q10	5.3547	13088.296594	2.654E-27	0.02380	183.97810	1.42E-02	1.39E-02	-2.15E-03	3.64E-03	3.22E-03
P10P10	5.5000	13090.061596	3.135E-27	0.02702	155.22743	1.43E-02	1.41E-02	-2.11E-03	3.64E-03	3.16E-03
P10Q9	4.8547	13091.995098	2.792E-27	0.02385	153.29393	1.43E-02	1.41E-02	-2.11E-03	3.58E-03	3.16E-03
P9P9	5.0000	13093.659535	3.262E-27	0.02746	127.33895	1.45E-02	1.43E-02	-2.07E-03	3.57E-03	3.08E-03
P9Q8	4.3547	13095.604765	2.867E-27	0.02391	125.39372	1.45E-02	1.43E-02	-2.07E-03	3.51E-03	3.08E-03
P8P8	4.5000	13097.167946	3.316E-27	0.02802	102.23621	1.47E-02	1.45E-02	-2.02E-03	3.47E-03	3.00E-03
P8Q7	3.8548	13099.125864	2.866E-27	0.02399	100.27830	1.47E-02	1.45E-02	-2.02E-03	3.43E-03	3.00E-03
P7P7	4.0000	13100.586813	3.284E-27	0.02874	79.92020	1.50E-02	1.47E-02	-1.98E-03	3.37E-03	2.91E-03
P7Q6	3.3548	13102.558824	2.779E-27	0.02410	77.94819	1.50E-02	1.47E-02	-1.98E-03	3.34E-03	2.91E-03
P6P6	3.5000	13103.916109	3.158E-27	0.02972	60.39178	1.53E-02	1.50E-02	-1.94E-03	3.24E-03	2.80E-03
P6Q5	2.8549	13105.904385	2.600E-27	0.02424	58.40350	1.53E-02	1.50E-02	-1.94E-03	3.23E-03	2.80E-03
P5P5	3.0000	13107.155796	2.936E-27	0.03114	43.65172	1.57E-02	1.53E-02	-1.90E-03	3.08E-03	2.68E-03
P5Q4	2.3551	13109.163968	2.326E-27	0.02444	41.64354	1.57E-02	1.53E-02	-1.90E-03	3.10E-03	2.68E-03
P4P4	2.5000	13110.305822	2.617E-27	0.03337	29.70066	1.61E-02	1.57E-02	-1.85E-03	2.90E-03	2.53E-03
P4Q3	1.8555	13112.340671	1.961E-27	0.02477	27.66582	1.61E-02	1.57E-02	-1.85E-03	2.93E-03	2.53E-03
P3P3	2.0000	13113.366126	2.210E-27	0.03738	18.53917	1.67E-02	1.62E-02	-1.81E-03	2.67E-03	2.36E-03
P3Q2	1.3563	13115.442748	1.513E-27	0.02535	16.46255	1.67E-02	1.62E-02	-1.81E-03	2.74E-03	2.36E-03
P2P2	1.5000	13116.336633	1.725E-27	0.04673	10.16767	1.73E-02	1.67E-02	-1.77E-03	2.39E-03	2.15E-03
P2Q1	0.8597	13118.502056	9.990E-28	0.02678	8.00224	1.73E-02	1.67E-02	-1.77E-03	2.49E-03	2.15E-03
P1P1	1.0000	13119.217258	1.182E-27	0.09347	4.58648	1.82E-02	1.74E-02	-1.72E-03	2.03E-03	1.89E-03
R0Q1	0.6403	13126.504300	7.728E-28	0.01995	0.00000	1.73E-02	1.67E-02	-1.77E-03	4.38E-03	2.15E-03
R1R1	0.5000	13127.318812	5.902E-28	0.00935	4.58648	1.67E-02	1.62E-02	-1.81E-03	4.42E-03	2.36E-03
R1Q2	1.1437	13129.203464	1.362E-27	0.02138	2.70183	1.67E-02	1.62E-02	-1.81E-03	4.41E-03	2.36E-03

R2R2	1.0000	13129.838819	1.148E-27	0.01336	10.16767	1.61E-02	1.57E-02	-1.85E-03	4.46E-03	2.53E-03
R2Q3	1.6445	13131.765269	1.906E-27	0.02197	8.24122	1.61E-02	1.57E-02	-1.85E-03	4.45E-03	2.53E-03
R3R3	1.5000	13132.268342	1.654E-27	0.01559	18.53917	1.57E-02	1.53E-02	-1.90E-03	4.50E-03	2.68E-03
R3Q4	2.1449	13134.221497	2.386E-27	0.02229	16.58601	1.57E-02	1.53E-02	-1.90E-03	4.47E-03	2.68E-03
R4R4	2.0000	13134.607224	2.088E-27	0.01700	29.70066	1.53E-02	1.50E-02	-1.94E-03	4.53E-03	2.80E-03
R4Q5	2.6451	13136.580313	2.787E-27	0.02249	27.72757	1.53E-02	1.50E-02	-1.94E-03	4.49E-03	2.80E-03
R5R5	2.5000	13136.855296	2.438E-27	0.01799	43.65172	1.50E-02	1.47E-02	-1.98E-03	4.56E-03	2.91E-03
R5Q6	3.1452	13138.844696	3.096E-27	0.02263	41.66232	1.50E-02	1.47E-02	-1.98E-03	4.51E-03	2.91E-03
R6R6	3.0000	13139.012382	2.696E-27	0.01871	60.39178	1.47E-02	1.45E-02	-2.02E-03	4.58E-03	3.00E-03
R6Q7	3.6452	13141.015927	3.307E-27	0.02273	58.38823	1.47E-02	1.45E-02	-2.02E-03	4.52E-03	3.00E-03
R7R7	3.5000	13141.078288	2.860E-27	0.01926	79.92020	1.45E-02	1.43E-02	-2.07E-03	4.60E-03	3.08E-03
R7Q8	4.1453	13143.094581	3.419E-27	0.02281	77.90391	1.45E-02	1.43E-02	-2.07E-03	4.53E-03	3.08E-03
R8R8	4.0000	13143.052814	2.931E-27	0.01969	102.23621	1.43E-02	1.41E-02	-2.11E-03	4.62E-03	3.16E-03
R8Q9	4.6453	13145.080902	3.437E-27	0.02287	100.20813	1.43E-02	1.41E-02	-2.11E-03	4.54E-03	3.16E-03
R9R9	4.5000	13144.935744	2.918E-27	0.02004	127.33895	1.42E-02	1.39E-02	-2.15E-03	4.63E-03	3.22E-03
R9Q10	5.1453	13146.974947	3.369E-27	0.02292	125.29975	1.42E-02	1.39E-02	-2.15E-03	4.55E-03	3.22E-03
R10R10	5.0000	13146.726853	2.831E-27	0.02033	155.22743	1.40E-02	1.38E-02	-2.18E-03	4.64E-03	3.29E-03
R10Q11	5.6454	13148.776671	3.227E-27	0.02296	153.17761	1.40E-02	1.38E-02	-2.18E-03	4.56E-03	3.29E-03
R11R11	5.5000	13148.425903	2.682E-27	0.02058	185.90056	1.39E-02	1.36E-02	-2.22E-03	4.66E-03	3.34E-03
R11Q12	6.1454	13150.485957	3.026E-27	0.02300	183.84051	1.39E-02	1.36E-02	-2.22E-03	4.57E-03	3.34E-03
R12R12	6.0000	13150.032645	2.486E-27	0.02079	219.35715	1.37E-02	1.35E-02	-2.26E-03	4.67E-03	3.40E-03
R12Q13	6.6454	13152.102641	2.781E-27	0.02303	217.28715	1.37E-02	1.35E-02	-2.26E-03	4.58E-03	3.40E-03
R13R13	6.5000	13151.546817	2.258E-27	0.02097	255.59588	1.36E-02	1.33E-02	-2.30E-03	4.68E-03	3.46E-03
R13Q14	7.1454	13153.626524	2.507E-27	0.02305	253.51617	1.36E-02	1.33E-02	-2.30E-03	4.59E-03	3.46E-03
R14R14	7.0000	13152.968148	2.011E-27	0.02112	294.61534	1.34E-02	1.32E-02	-2.33E-03	4.69E-03	3.51E-03
R14Q15	7.6454	13155.057378	2.218E-27	0.02307	292.52611	1.34E-02	1.32E-02	-2.33E-03	4.59E-03	3.51E-03
R15R15	7.5000	13154.296352	1.758E-27	0.02126	336.41400	1.32E-02	1.30E-02	-2.37E-03	4.71E-03	3.57E-03
R15Q16	8.1454	13156.394954	1.929E-27	0.02309	334.31540	1.32E-02	1.30E-02	-2.37E-03	4.60E-03	3.57E-03
R16R16	8.0000	13155.531133	1.510E-27	0.02138	380.99023	1.30E-02	1.29E-02	-2.40E-03	4.72E-03	3.63E-03
R16Q17	8.6454	13157.638984	1.648E-27	0.02311	378.88238	1.30E-02	1.29E-02	-2.40E-03	4.61E-03	3.63E-03
R17R17	8.5000	13156.672184	1.274E-27	0.02149	428.34229	1.28E-02	1.27E-02	-2.44E-03	4.74E-03	3.70E-03
R17Q18	9.1454	13158.789179	1.385E-27	0.02312	426.22529	1.28E-02	1.27E-02	-2.44E-03	4.63E-03	3.70E-03
R18R18	9.0000	13157.719185	1.057E-27	0.02158	478.46832	1.26E-02	1.25E-02	-2.47E-03	4.76E-03	3.76E-03
R18Q19	9.6454	13159.845237	1.144E-27	0.02314	476.34226	1.26E-02	1.25E-02	-2.47E-03	4.64E-03	3.76E-03
R19R19	9.5000	13158.671805	8.625E-28	0.02167	531.36635	1.23E-02	1.23E-02	-2.50E-03	4.78E-03	3.84E-03
R19Q20	10.1454	13160.806841	9.306E-28	0.02315	529.23132	1.23E-02	1.23E-02	-2.50E-03	4.65E-03	3.84E-03
R20R20	10.0000	13159.529702	6.925E-28	0.02175	587.03433	1.21E-02	1.21E-02	-2.54E-03	4.81E-03	3.91E-03
R20Q21	10.6454	13161.673658	7.449E-28	0.02316	584.89037	1.21E-02	1.21E-02	-2.54E-03	4.67E-03	3.91E-03
R21R21	10.5000	13160.292519	5.473E-28	0.02182	645.47007	1.18E-02	1.19E-02	-2.57E-03	4.83E-03	3.99E-03
R21Q22	11.1454	13162.445343	5.870E-28	0.02317	643.31724	1.18E-02	1.19E-02	-2.57E-03	4.68E-03	3.99E-03
R22R22	11.0000	13160.959892	4.257E-28	0.02188	706.67127	1.15E-02	1.17E-02	-2.60E-03	4.86E-03	4.08E-03
R22Q23	11.6454	13163.121537	4.554E-28	0.02317	704.50963	1.15E-02	1.17E-02	-2.60E-03	4.70E-03	4.08E-03
R23R23	11.5000	13161.531442	3.261E-28	0.02194	770.63555	1.11E-02	1.15E-02	-2.63E-03	4.89E-03	4.16E-03
R23Q24	12.1454	13163.701868	3.480E-28	0.02318	768.46513	1.11E-02	1.15E-02	-2.63E-03	4.72E-03	4.16E-03
R24R24	12.0000	13162.006779	2.460E-28	0.02200	837.36040	1.08E-02	1.12E-02	-2.66E-03	4.91E-03	4.25E-03
R24Q25	12.6454	13164.185952	2.620E-28	0.02319	835.18123	1.08E-02	1.12E-02	-2.66E-03	4.74E-03	4.25E-03
R25R25	12.5000	13162.385503	1.828E-28	0.02205	906.84320	1.05E-02	1.10E-02	-2.69E-03	4.94E-03	4.34E-03
R25Q26	13.1454	13164.573392	1.942E-28	0.02319	904.65531	1.05E-02	1.10E-02	-2.69E-03	4.76E-03	4.34E-03

R26R26	13.0000	13162.667199	1.338E-28	0.02209	979.08123	1.01E-02	1.08E-02	-2.71E-03	4.97E-03	4.43E-03
R26Q27	13.6454	13164.863780	1.419E-28	0.02320	976.88465	1.01E-02	1.08E-02	-2.71E-03	4.77E-03	4.43E-03
R27R27	13.5000	13162.851444	9.646E-29	0.02213	1054.07165	9.83E-03	1.05E-02	-2.74E-03	5.00E-03	4.52E-03
R27Q28	14.1454	13165.056692	1.022E-28	0.02320	1051.86640	9.83E-03	1.05E-02	-2.74E-03	4.79E-03	4.52E-03
R28R28	14.0000	13162.937800	6.855E-29	0.02217	1131.81152	9.52E-03	1.03E-02	-2.77E-03	5.02E-03	4.61E-03
R28Q29	14.6454	13165.151696	7.249E-29	0.02320	1129.59762	9.52E-03	1.03E-02	-2.77E-03	4.81E-03	4.61E-03
R29R29	14.5000	13162.925820	4.800E-29	0.02221	1212.29779	9.23E-03	1.01E-02	-2.79E-03	5.05E-03	4.69E-03
R29Q30	15.1454	13165.148346	5.069E-29	0.02321	1210.07526	9.23E-03	1.01E-02	-2.79E-03	4.82E-03	4.69E-03
R30R30	15.0000	13162.815044	3.313E-29	0.02224	1295.52730	8.96E-03	9.89E-03	-2.82E-03	5.07E-03	4.77E-03
R30Q31	15.6454	13165.046185	3.494E-29	0.02321	1293.29615	8.96E-03	9.89E-03	-2.82E-03	4.84E-03	4.77E-03
R31R31	15.5000	13162.605000	2.254E-29	0.02227	1381.49677	8.70E-03	9.69E-03	-2.84E-03	5.09E-03	4.85E-03
R31Q32	16.1454	13164.844743	2.374E-29	0.02321	1379.25703	8.70E-03	9.69E-03	-2.84E-03	4.85E-03	4.85E-03
R32R32	16.0000	13162.295205	1.512E-29	0.02230	1470.20284	8.46E-03	9.50E-03	-2.87E-03	5.11E-03	4.92E-03
R32Q33	16.6454	13164.543538	1.590E-29	0.02321	1467.95451	8.46E-03	9.50E-03	-2.87E-03	4.87E-03	4.92E-03
R33R33	16.5000	13161.885164	9.993E-30	0.02233	1561.64201	8.24E-03	9.32E-03	-2.89E-03	5.13E-03	4.99E-03
R33Q34	17.1454	13164.142076	1.050E-29	0.02321	1559.38510	8.24E-03	9.32E-03	-2.89E-03	4.88E-03	4.99E-03
R34R34	17.0000	13161.374371	6.514E-30	0.02235	1655.81069	8.04E-03	9.15E-03	-2.91E-03	5.15E-03	5.05E-03
R34Q35	17.6454	13163.639853	6.837E-30	0.02321	1653.54521	8.04E-03	9.15E-03	-2.91E-03	4.89E-03	5.05E-03
R35R35	17.5000	13160.762306	4.186E-30	0.02237	1752.70517	7.86E-03	9.00E-03	-2.94E-03	5.16E-03	5.11E-03
R35Q36	18.1454	13163.036352	4.390E-30	0.02321	1750.43112	7.86E-03	9.00E-03	-2.94E-03	4.90E-03	5.11E-03
R36R36	18.0000	13160.048441	2.653E-30	0.02240	1852.32164	7.70E-03	8.85E-03	-2.96E-03	5.18E-03	5.17E-03
R36Q37	18.6454	13162.331043	2.779E-30	0.02321	1850.03903	7.70E-03	8.85E-03	-2.96E-03	4.91E-03	5.17E-03
R37R37	18.5000	13159.232232	1.658E-30	0.02241	1954.65617	7.55E-03	8.72E-03	-2.98E-03	5.19E-03	5.22E-03
R37Q38	19.1454	13161.523386	1.735E-30	0.02321	1952.36501	7.55E-03	8.72E-03	-2.98E-03	4.92E-03	5.22E-03
R38R38	19.0000	13158.313128	1.022E-30	0.02243	2059.70473	7.41E-03	8.59E-03	-3.00E-03	5.20E-03	5.27E-03
R38Q39	19.6454	13160.612828	1.069E-30	0.02321	2057.40503	7.41E-03	8.59E-03	-3.00E-03	4.92E-03	5.27E-03
R39R39	19.5000	13157.290562	6.211E-31	0.02245	2167.46318	7.29E-03	8.48E-03	-3.02E-03	5.21E-03	5.31E-03
R39Q40	20.1454	13159.598804	6.490E-31	0.02320	2165.15494	7.29E-03	8.48E-03	-3.02E-03	4.93E-03	5.31E-03
R40R40	20.0000	13156.163959	3.723E-31	0.02246	2277.92727	7.17E-03	8.38E-03	-3.04E-03	5.22E-03	5.35E-03
R40Q41	20.6454	13158.480739	3.888E-31	0.02320	2275.61049	7.17E-03	8.38E-03	-3.04E-03	4.94E-03	5.35E-03

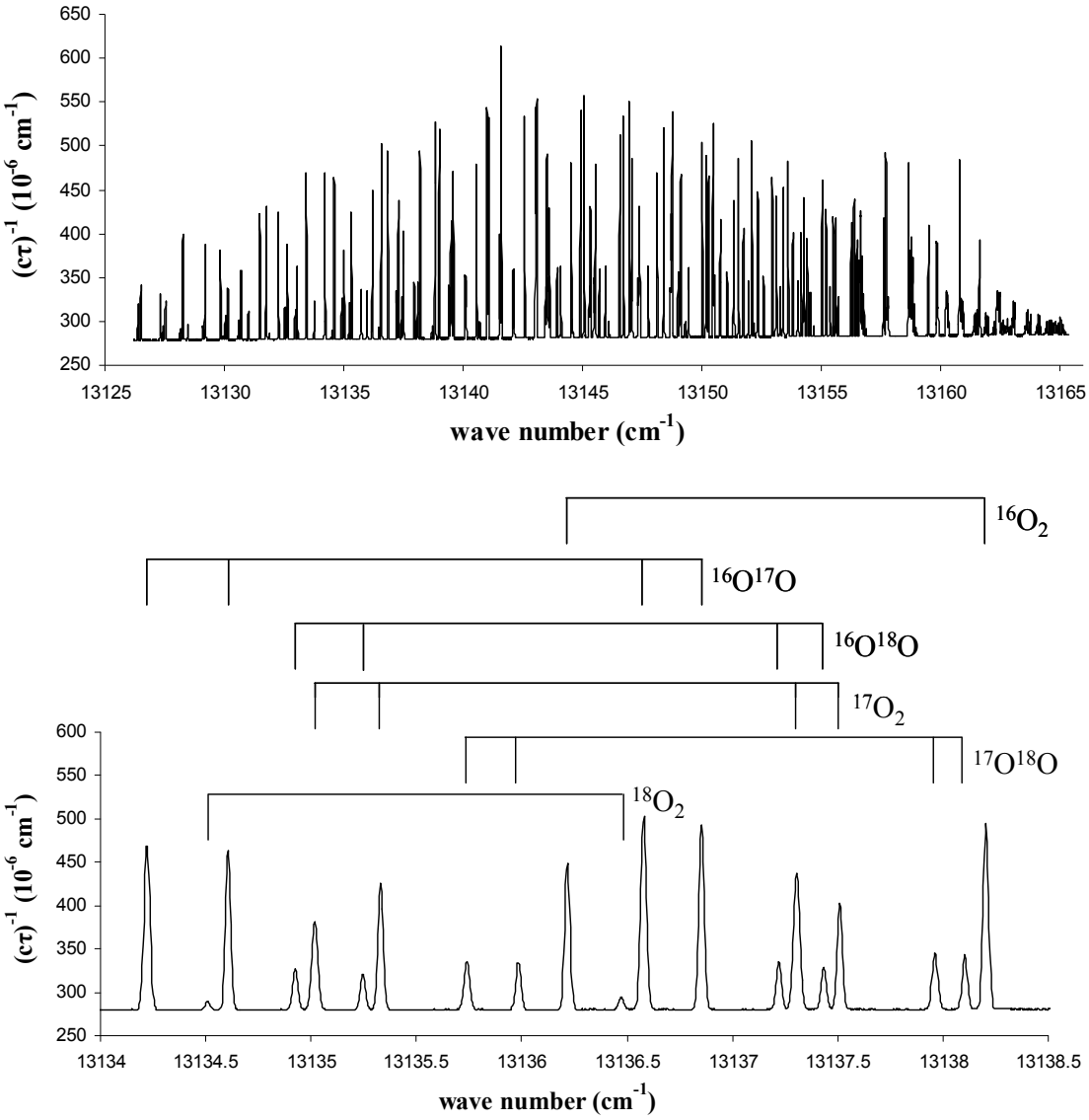

Figure 1. Upper panel: Recorded absorption spectrum of the *R*-branch of the O_2 *A*-band at 0.234 kPa (1.75 Torr) ^{17}O-enriched gas (see Table 1 for composition) at 299.5 K. Lower panel: The above scan between 13134.0-13138.5 cm^{-1} with isotopologue assignments shown.

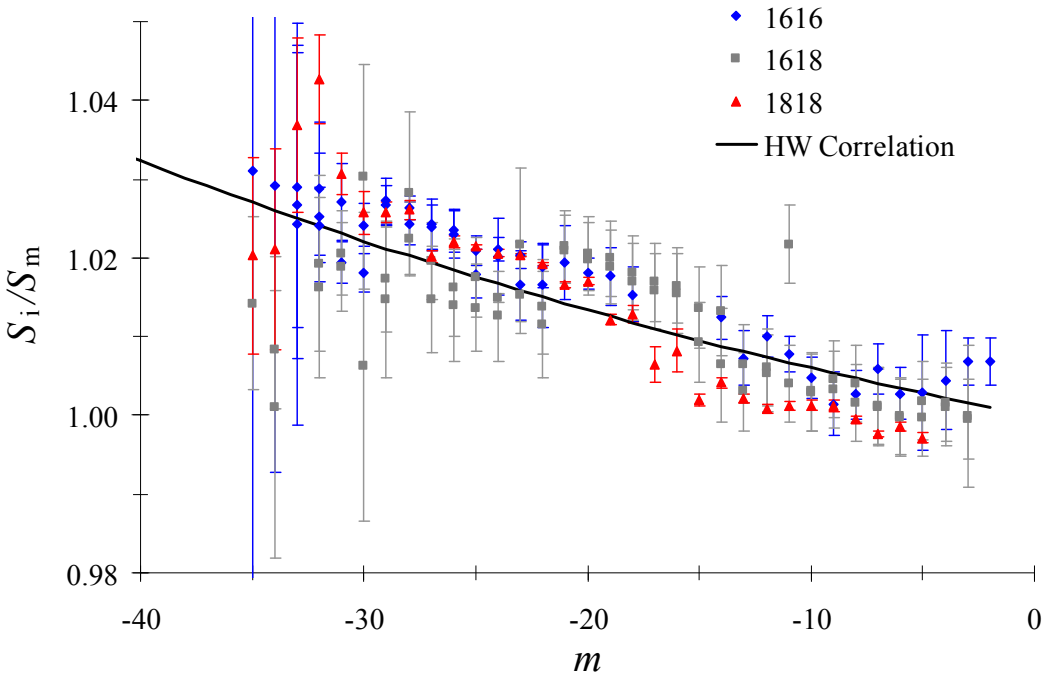

Figure 2. Comparison of measured FS-CRDS intensities (S_i) to intensities calculated using the standard model of Gamache et al. [47] with the Hönl-London factors of Watson [48] (S_m) for the $^{16}O_2$, $^{16}O^{18}O$, and $^{18}O_2$ isotopologues. Also shown is a quadratic Herman-Wallis (HW) correlation [44] of the form $F=(1+a_1m+a_2m^2)^2$ where a_1 and a_2 were determined via a fit to the $^{16}O_2$ measurements to be -2.6580×10^{-4} and 3.3622×10^{-6}, respectively. As can be seen, this correlation matches the $^{16}O^{18}O$ and $^{18}O_2$ measurements to within the experimental uncertainty.

Appendix A: Supplementary Material

Table S1. Measured $^{16}O^{17}O$ (1617) line positions, uncertainties (Unc), and the difference between observed line positions (Obs) and those calculated (Calc) using the parameters found in Tables 2 and 3. All measurements were made on the ^{17}O-enriched sample (see Table 1 for isotopic composition).

Assignment $\Delta N\ N''\ \Delta J\ J''$	Position (cm^{-1})	Unc (10^{-5} cm^{-1})	Obs-Calc (10^{-5} cm^{-1})	Sample
R0Q1	13126.50416	25	-14	17
R1R1	13127.31879	25	-2	17
R1Q2	13129.20387	25	41	17
R2R2	13129.83936	25	54	17
R3Q4	13134.22093	24	-57	17
R4R4	13134.60675	24	-48	17
R4Q5	13136.58025	24	-6	17
R5R5	13136.85489	24	-41	17
R5Q6	13138.84470	24	1	17
R6R6	13139.01246	24	7	17
R6Q7	13141.01599	48	7	17
R7R7	13141.07838	48	9	17
R8R8	13143.05334	48	52	17
R7Q8	13143.09510	48	52	17
R9R9	13144.93589	24	14	17
R8Q9	13145.08106	24	16	17
R10R10	13146.72690	24	4	17
R9Q10	13146.97505	24	11	17
R11R11	13148.42558	24	-33	17
R10Q11	13148.77642	72	-25	17
R12R12	13150.03266	24	1	17
R11Q12	13150.48610	48	15	17
R13R13	13151.54712	24	30	17
R12Q13	13152.10239	24	-25	17
R14R14	13152.96802	24	-13	17
R13Q14	13153.62646	24	-6	17
R15R15	13154.29624	48	-12	17
R14Q15	13155.05754	24	16	17
R16R16	13155.53118	24	4	17
R15Q16	13156.39490	24	-5	17

Table S2. Measured $^{16}O^{18}O$ (1618) line positions, uncertainties (Unc), and the difference between observed line positions (Obs) and those calculated (Calc) using the parameters found in Tables 2 and 3. Measurements were made on either the ^{17}O-enriched (17) or ^{18}O-enriched (18) sample (see Table 1 for isotopic compositions).

Assignment $\Delta N\ N''\ \Delta J\ J''$	Position (cm^{-1})	Unc (10^{-5} cm^{-1})	Obs-Calc (10^{-5} cm^{-1})	Sample
R0Q1	13127.42102	24	-19	18
R1R1	13128.15250	24	-2	18
R1Q2	13130.04493	24	37	18
R2R2	13130.60487	24	-12	18
R2Q3	13132.53661	24	28	18
R3R3	13132.96980	24	34	18
R3Q4	13134.92577	24	-26	18
R4R4	13135.24562	24	-17	18
R4Q5	13137.22106	24	-22	18
R5R5	13137.43362	24	-19	18
R5Q6	13139.42508	24	24	18
R6R6	13139.53362	24	28	18
R8R8	13143.46604	48	-19	17
R7Q8	13143.56077	72	-22	17
R9R9	13145.29942	47	25	17
R8Q9	13145.49450	48	16	17
R10R10	13147.04291	72	7	17
R9Q10	13147.33810	72	12	17
R11R11	13148.69669	72	-29	17
R10Q11	13149.09159	72	-29	17

Table S3. Measured $^{17}O^{17}O$ (1717) line positions, uncertainties (Unc), and the difference between observed line positions (Obs) and those calculated (Calc) using the parameters found in Tables 2 and 3. All measurements were made on the ^{17}O-enriched sample (see Table 1 for isotopic composition).

Assignment $\Delta N\ N''\ \Delta J\ J''$	Position (cm^{-1})	Unc (10^{-5} cm^{-1})	Obs-Calc (10^{-5} cm^{-1})	Sample
R1Q2	13130.15582	25	118	17
R2R2	13130.70447	24	-84	17
R2Q3	13132.63690	24	-40	17
R3R3	13133.06098	24	-37	17
R3Q4	13135.01845	24	8	17
R4R4	13135.32964	24	6	17
R4Q5	13137.30543	24	4	17
R5R5	13137.50982	24	-2	17
R5Q6	13139.50152	72	43	17
R6R6	13139.60232	24	36	17
R8R8	13143.52076	48	-26	17
R7Q8	13143.62248	48	-12	17
R9R9	13145.34761	24	6	17
R8Q9	13145.54933	24	20	17
R10R10	13147.08496	48	-15	17
R9Q10	13147.38627	72	-4	17
R11R11	13148.73287	72	-61	17
R10Q11	13149.13360	48	-46	17
R11Q12	13150.79213	72	-13	17
R12Q13	13152.36039	72	-34	17
R14R14	13153.14054	72	-25	17
R13Q14	13153.83907	72	-20	17
R14Q15	13155.22859	73	94	17

Table S4. Measured $^{17}O^{18}O$ (1718) line positions, uncertainties (Unc), and the difference between observed line positions (Obs) and those calculated (Calc) using the parameters found in Tables 2 and 3. All measurements were made on the ^{17}O-enriched sample (see Table 1 for isotopic composition).

Assignment $\Delta N\ N''\ \Delta J\ J''$	Position (cm^{-1})	Unc (10^{-5} cm^{-1})	Obs-Calc (10^{-5} cm^{-1})	Sample
R0Q1	13128.47552	26	44	17
R1R1	13129.11188	26	45	17
R1Q2	13131.01134	25	-103	17
R2Q3	13133.42487	101	10	17
R3R3	13133.77793	24	-52	17
R3Q4	13135.73912	24	-4	17
R4R4	13135.98394	24	-7	17
R4Q5	13137.96239	24	-5	17
R5R5	13138.10400	24	-8	17
R5Q6	13140.09715	48	0	17
R6R6	13140.13850	48	0	17
R7R7	13142.08746	48	36	17
R6Q7	13142.14478	48	41	17
R8R8	13143.94964	24	-5	17
R7Q8	13144.10457	24	0	17
R9R9	13145.72637	24	28	17
R8Q9	13145.97833	24	37	17
R9Q10	13147.76485	24	28	17
R11R11	13149.01928	24	-20	17
R10Q11	13149.46426	24	-11	17
R12R12	13150.53621	72	17	17
R11Q12	13151.07750	24	28	17
R13R13	13151.96521	24	-32	17
R12Q13	13152.60288	24	-12	17
R14R14	13153.30771	24	0	17
R13Q14	13154.04153	24	2	17
R15R15	13154.56239	24	6	17
R14Q15	13155.39282	24	27	17
R16R16	13155.72892	24	-19	17

Table S5. Measured $^{18}O^{18}O$ (1818) line positions, uncertainties (Unc), and the difference between observed line positions (Obs) and those calculated (Calc) using the parameters found in Tables 2 and 3. Measurements were made on either the ^{17}O-enriched (17) or ^{18}O-enriched (18) sample (see Table 1 for isotopic compositions).

Assignment $\Delta N\ N''\ \Delta J\ J''$	Position (cm^{-1})	Unc (10^{-5} cm^{-1})	Obs-Calc (10^{-5} cm^{-1})	Sample
R1R1	13129.97558	24	33	18
R1Q2	13131.88468	24	11	18
R3R3	13134.50922	24	-35	18
R3Q4	13136.47434	24	9	18
R5R5	13138.71252	24	7	18
R5Q6	13140.70756	24	2	18
R7Q8	13144.60107	49	10	17
R9R9	13146.11954	26	49	17
R11R11	13149.31970	26	-25	17
R13R13	13152.18353	26	-23	17
R13Q14	13154.25810	73	-2	17
R15R15	13154.70863	28	-4	17
R17R17	13156.89267	29	-3	17